

Entropy Guided Dynamic Patch Segmentation for Time Series Transformers

Sachith Abeywickrama^{1,2} Emadeldeen Eldele^{3,2} Min Wu² Xiaoli Li^{2,4} Chau Yuen¹

Abstract

Patch-based transformers have emerged as efficient and improved long-horizon modeling architectures for time series modeling. Yet, existing approaches rely on *temporally-agnostic* patch construction, where arbitrary starting positions and fixed lengths fracture temporal coherence by splitting natural transitions across boundaries. This naive segmentation often disrupts short-term dependencies and weakens representation learning. We propose a novel **Entropy-Guided Dynamic Patch Encoder (EntroPE)**, as a temporally informed framework that dynamically detects transition points via conditional entropy and dynamically places patch boundaries. This preserves temporal structure while retaining the computational benefits of patching. EntroPE consists of two key modules, namely an **Entropy-based Dynamic Patcher (EDP)** that applies information-theoretic criteria to locate natural temporal shifts and determine patch boundaries, and an **Adaptive Patch Encoder (APE)** that employs pooling and cross-attention to capture intra-patch dependencies and produce fixed-size latent representations. Extensive experiments on long-term forecasting, classification, and anomaly detection demonstrate that the proposed method improves both accuracy and efficiency, establishing entropy-guided dynamic patching as a promising new paradigm for time series modeling.

1. Introduction

Time series analysis is fundamental to numerous critical applications, including electricity load forecasting (Gasparin et al., 2022), financial market prediction (Fischer & Krauss,

¹School of Electrical and Electronic Engineering, Nanyang Technological University, Singapore ²Institute for Infocomm Research, A*STAR, Singapore ³Department of Computer Science, Khalifa University, UAE ⁴Information Systems Technology and Design, Singapore University of Technology and Design, Singapore. Correspondence to: Emadeldeen Eldele <emad0002@ntu.edu.sg>.

Preprint. January 30, 2026.

(a) Temporally-agnostic Patching: Patch boundaries are placed without regard to temporal coherence, leading to heterogeneous fragmentation of patterns.



(b) Temporally-informed Patching: Patch boundaries lie at natural transition points where the entropy is high.

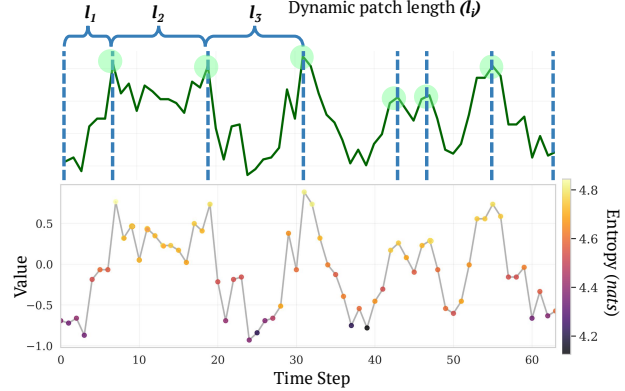


Figure 1. Comparison of patching strategies. (a) Temporally-agnostic fixed-length patching places boundaries at arbitrary positions, fragmenting coherent temporal patterns (highlighted regions show split transitions). (b) Our temporally-informed approach places boundaries at entropy peaks, where conditional entropy scale indicates natural transition points, preserving temporal coherence within patches.

2018), healthcare monitoring (Reis & Mandl, 2003), and environmental surveillance (Smith, 1989). However, accurately modeling time series data remains challenging due to inherent noise, complex temporal dependencies, and irregular patterns spanning multiple time horizons (Lim & Zohren, 2021; Torres et al., 2021). The transformer architecture (Vaswani et al., 2017) has revolutionized language and sequence modeling across domains through self-attention mechanisms, leading to significant advances in time series analysis. Despite their promise in learning long-term temporal relationships, time series transformers remain suboptimal due to unique complexities such as non-stationarity, seasonality, varying temporal granularities (Wen et al., 2023; Zeng et al., 2023).

Recent advances in time series transformers include Informer (Zhou et al., 2021), Autoformer (Wu et al., 2021), and FEDformer (Zhou et al., 2022), which address long-sequence modeling challenges through sparse attention mechanisms, decomposition techniques, and improved positional encodings while operating on point-wise inputs. Triformer (Cirstea et al., 2022) and PatchTST (Nie et al., 2023) introduced a patch-based input representation, dividing raw sequences into fixed-length patches and achieving substantial improvements in computational efficiency and performance. This demonstrated the critical impact of input tokenization strategies on transformer performance in time series. However, subsequent approaches have predominantly adopted similar *temporally-agnostic* patching schemes, which may not fully capture the temporal coherence and statistical properties inherent in time series data.

These patching strategies treat time as temporally-homogeneous, partitioning sequences at arbitrary positions without regard for underlying temporal structure. *Temporally-agnostic* patching introduces two fundamental challenges. They create inconsistent input representations between training and inference phases. While training observes patches starting at diverse temporal offsets, result in patches that begin at various temporal positions relative to underlying patterns (e.g., a patch might start mid-trend in one sample but at a trend beginning in another). However, during inference, patches are extracted from predetermined positions in the input sequence, creating a systematic distribution shift in patch configurations. Further, predetermined patch boundaries arbitrarily segment coherent temporal structures without regard for frequent underlying dynamics (see Fig. 1(a)). For example, a frequently occurring gradual trend change or seasonal transition may be split across multiple patches, breaking the natural temporal dependencies that are crucial for accurate pattern recognition.

These challenges directly impact model performance. Fragmented temporal patterns lead to incomplete intra-patch representations, where semantically related time points are separated across different patches and processed independently. Additionally, the train-inference mismatch reduces the model’s ability to generalize, as it must extrapolate to patch configurations with different statistical properties than those encountered during training. This is particularly detrimental for capturing rapid transitions and fine-grained temporal dynamics that require consistent temporal context.

We argue that patch boundaries should align with points of elevated **predictive uncertainty**, where the past provides insufficient information to determine the future. Formally, such moments are characterized by high conditional entropy of the next observation given historical context. Segmenting time at these entropy peaks localizes regime changes at patch boundaries while yielding patches whose

interiors remain predictively coherent. Motivated by this principle, we introduce EntroPE, an **Entropy-Guided Dynamic Patch Encoder**, which integrates *uncertainty-aware* boundary detection as a core architectural component. Unlike prior approaches that fix patch length or rely on heuristic change-point detectors, EntroPE derives segmentation from information-theoretic predictive structure, ensuring patch boundaries align with natural temporal transitions (Fig. 1(b)). We then employ adaptive encoding mechanisms to process these variable-length patches while preserving intra-patch dependencies. This temporally-informed approach addresses both the train-inference mismatch and boundary fragmentation issues inherent in *temporally-agnostic* patching methods.

The main contributions of this paper are:

- We propose EntroPE, the first information-theoretic framework for dynamic patching in time series transformers.
- We introduce an adaptive segmentation mechanism that balances modeling accuracy and attention complexity by dynamically controlling patch resolution.
- We demonstrate consistent improvements across forecasting, classification, and anomaly detection, establishing entropy-guided dynamic patching as a practical and generalizable paradigm for time series analysis.

Code is publicly available at <https://github.com/Sachithx/EntroPE>.

2. Related Work

Transformers have significantly advanced time series modeling by enabling long-range dependency learning through self-attention. Early adaptations such as Informer (Zhou et al., 2021), Autoformer (Wu et al., 2021), and FEDformer (Zhou et al., 2022) improved scalability via sparse attention, decomposition, and frequency-domain modeling. However, these approaches operate on point-wise tokens, resulting in prohibitively long sequences and a fundamental trade-off between temporal resolution and computational tractability.

Patch-Based Input Representations. Inspired by Vision Transformers (Dosovitskiy et al., 2021), patch-based methods reduce sequence length while preserving local temporal semantics. Triformer (Cirstea et al., 2022) and PatchTST (Nie et al., 2023) pioneered fixed-length temporal patching, demonstrating substantial gains in efficiency and forecasting accuracy. Subsequent work extended this paradigm through hierarchical dependency modeling (Crossformer (Zhang & Yan, 2023)), multivariate forecasting adaptation (CARD (Xue et al., 2024)), and patch-independent self-supervised learning (Lee et al., 2024). Beyond transformers, xPatch

(Stitsyuk & Choi, 2025), Pathformer (Chen et al., 2024), and PatchMLP (Tang & Zhang, 2025) explore CNN- and MLP-based hierarchical architectures to capture multi-scale temporal patterns.

Adaptive and Multi-Granularity Patching. Recent efforts relax fixed patch sizes through adaptive or multi-scale segmentation. MSPatch (Cao et al., 2025) employs multi-resolution patches, HDMixer (Huang et al., 2024) enables length-extendable interpolation, and MOIRAI (Woo et al., 2024) determines patch size in the frequency domain. AdaPatch (Liu et al., 2025a) mitigates non-stationarity via patch-level normalization and reconstruction, but operates over fixed segmentation rather than learning boundary placement. APN (Liu et al., 2025c) introduces time-aware adaptive patching for irregular time series through soft window aggregation, emphasizing data-density regularization instead of causality driven segmentation. SRSNet (Wu et al., 2025) constructs a selective representation space by scoring, selecting, and reassembling candidate patches, but operates over dense sliding-window patch pools rather than discovering causally meaningful boundary locations. TimeMosaic (Ding et al., 2025) further adapts patch granularity based on temporal heterogeneity and motif reuse, optimizing representation efficiency and decoding specialization through segment-wise prompting. While these methods improve flexibility, their segmentation criteria remain largely heuristic or representation-driven, prioritizing encoding density, frequency structure, or compression objectives over the underlying predictive or causal structure of the time series.

Causal and Information-Theoretic Perspectives on Segmentation. A complementary line of research argues that segmentation should reflect changes in predictive structure. In NLP, Byte Latent Transformer (Pagnoni et al., 2025) demonstrates that architecture-integrated dynamic tokenization improves efficiency by adapting token boundaries to information content. However, existing time series methods have not systematically grounded patch boundary selection in information-theoretic measures of predictive uncertainty or temporal causality.

In contrast to prior work that optimizes patching for representational efficiency or frequency structure, EntroPE places patch boundaries at peaks of conditional predictive entropy. This identifies moments where the past becomes insufficient to predict the future, typically corresponding to regime shifts or structural transitions. This principled segmentation preserves temporal coherence within patches, localizes uncertainty at boundaries, and eliminates train-inference patch mismatch. By coupling entropy-guided dynamic patching with adaptive encoding for variable-length segments, our method introduces a fundamentally new criterion for patch construction based on predictive uncertainty rather than heuristic granularity.

3. Method

3.1. Preliminaries: Problem Formulation

Given a multivariate time series $X = [x^{(1)}, \dots, x^{(C)}] \in \mathbb{R}^{C \times L}$ with C channels and look-back length L , we address three fundamental tasks, namely forecasting, classification, and anomaly detection. Following the channel-independence principle (Nie et al., 2023), our architecture f_ϕ processes each channel independently to obtain channel-wise representations $\mathbf{z}^{(c)} = f_\phi(x^{(c)})$ for $c = 1, \dots, C$. Here, f_ϕ encompasses the complete processing pipeline: entropy-guided dynamic patching, adaptive patch encoding, global transformer, and fusion decoder (detailed in Sec. 3.3-3.6), producing representations $Z = [\mathbf{z}^{(1)}, \dots, \mathbf{z}^{(C)}] \in \mathbb{R}^{C \times d}$ where d is the final representation dimension. Z is projected via linear layer based on specific task.

3.2. Overall Architecture

Our approach consists of two distinct phases (Fig. 2), (1) entropy model pre-training for uncertainty quantification, (2) task-specific training with entropy guided dynamic patching. Crucially, the entropy model parameters remain frozen during task-specific training, serving solely to provide patch boundaries.

3.3. Entropy Model Pre-training

As shown in Fig. 2(A), our dynamic patch boundary detection leverages a lightweight causal transformer to identify temporal transitions based on predictive uncertainty. Given a time series dataset $\mathcal{D}_{\text{pretrain}} = \{X^{(i)}\}_{i=1}^N$ where $X^{(i)} \in \mathbb{R}^{C \times L}$, we first quantize each continuous sequence into discrete tokens. For a univariate sequence $x = [x_1, \dots, x_L]$, we apply quantization $q : \mathbb{R} \rightarrow \mathcal{V}$ (defined in Eq. 38) to obtain tokenized sequence $\tau = [\tau_1, \dots, \tau_L]$ where $\tau_t = q(x_t) \in \mathcal{V}$ and $|\mathcal{V}| = V$.

A critical distinction. Unlike Chronos (Ansari et al., 2024), which operates entirely in the quantized domain and suffers from range limitations during dequantization, we use quantization only for computing entropies and input projection. The downstream prediction heads project the output-embeddings, not quantized tokens. This decoupling eliminates the quantization range constraint as our predictions are not limited to the discrete vocabulary. Quantization serves purely as a preprocessing step for the entropy model (Sec. 3.3), while the actual time series transformer and prediction heads operate on continuous representations throughout.

Determining Quantization Range. To avoid manual threshold selection, we determine bin boundaries $\{b_1, \dots, b_{V-1}\}$ from training data statistics. Let X_{train} denote z-score normalized training values. We compute em-

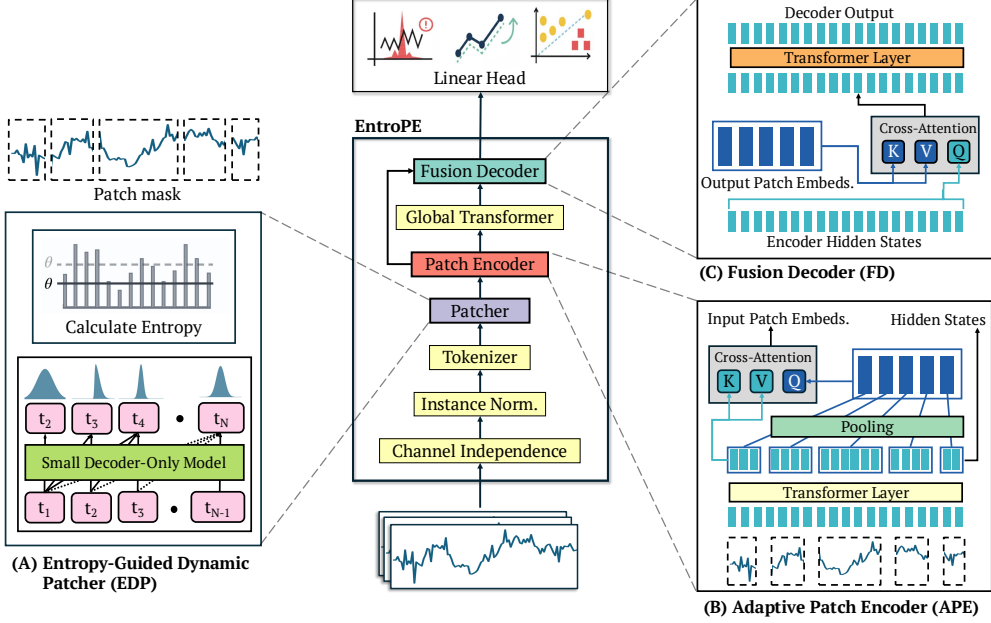


Figure 2. Comprehensive architecture of EntroPE. The model processes input through: (A) **Entropy-Based Dynamic Patcher** - A small causal transformer calculates entropy at each time point to identify boundaries where predictive uncertainty is high; (B) **Adaptive Patch Encoder** - Cross-attention layers aggregate intra-patch dependencies into fixed-size global embeddings; (C) **Fusion Decoder** - Cross-attention combines global patch context with local encoder hidden states for accurate predictions.

pirical quantiles:

$$q_{\text{low}} = Q_{\epsilon/2}(X_{\text{train}}), \quad q_{\text{high}} = Q_{1-\epsilon/2}(X_{\text{train}}) \quad (1)$$

where $\epsilon = 0.005$ captures 99.5% of the distribution. The symmetric quantization radius is $R = \max(|q_{\text{low}}|, |q_{\text{high}}|)$, and the interval $[-R, R]$ is uniformly divided into V bins.

Model Selection. Drawing inspiration from decoder-only transformers in time series (Das et al., 2024) and cross-entropy guided training in Chronos, we adopt the GPT-2 paradigm (Radford et al., 2019) to train a compact transformer for next-token prediction on quantized time series tokens. Our lightweight architecture comprises 8-16 embedding dimensions and 2 transformer layers, totaling $\approx 10k$ learnable parameters. The model performs autoregressive prediction at timesteps $\{t_2, t_3, \dots, t_L\}$ from input sequence $\{t_1, t_2, \dots, t_{L-1}\}$.

Model Training. We train our lightweight causal transformer $f_{\theta_{\text{ent}}} : \mathcal{V}^t \rightarrow \Delta^V$ (where Δ^V denotes the probability simplex over vocabulary \mathcal{V}) to perform next-token prediction. The model is optimized via:

$$\theta_{\text{ent}}^* = \arg \min_{\theta_{\text{ent}}} \mathbb{E}_{X \sim \mathcal{D}_{\text{pretrain}}} [\mathcal{L}_{\text{CE}}(X; \theta_{\text{ent}})] \quad (2)$$

where $\mathcal{L}_{\text{CE}}(X; \theta_{\text{ent}})$ is the cross-entropy loss (Eq. 21).

Once converged, we freeze θ_{ent}^* and use it exclusively for entropy computation, *not* for prediction or token generation.

This decoupling is critical, as the entropy model learns predictive uncertainty patterns, while downstream task models operate on continuous representations.

3.4. Entropy-Guided Dynamic Patcher (EDP)

Entropy Computation. For a new input sequence $X \in \mathbb{R}^{C \times L}$, we process each channel independently. For channel c , we compute the quantized sequence $\tau^{(c)} = [q(x_1^{(c)}), \dots, q(x_L^{(c)})]$ and use the frozen model θ_{ent}^* to calculate conditional entropy at each position:

$$H(x_t^{(c)}; \theta_{\text{ent}}^*) = - \sum_{v \in \mathcal{V}} p_{\theta_{\text{ent}}^*}(\tau_{t+1}^{(c)} = v | \tau_{\leq t}^{(c)}) \log p_{\theta_{\text{ent}}^*}(\tau_{t+1}^{(c)} = v | \tau_{\leq t}^{(c)}) \quad (3)$$

yielding entropy sequence,

$$\mathbf{H}^{(c)} = [H(x_1^{(c)}), \dots, H(x_L^{(c)})] \in \mathbb{R}^L. \quad (4)$$

As established in Appendix A.2, high conditional entropy indicates positions where the future is less predictable from the past, typically at regime shifts, trend reversals, or volatility bursts. By placing boundaries at such points (Proposition A.2), patches become internally coherent while transition uncertainty is localized at edges.

Adaptive Threshold Determination. Rather than using fixed global thresholds requiring manual tuning, we em-

ploy *sample-adaptive* thresholds derived from quantile-based estimation. For each input sequence with entropies $\{H(x_1^{(c)}), \dots, H(x_L^{(c)})\}$, we compute sample-specific thresholds. Hence, the threshold selection becomes interpretable.

The absolute entropy threshold is the α -th quantile of the sequence’s entropy distribution:

$$\theta_{\text{abs}}^{(c)} = Q_\alpha(\mathbf{H}^{(c)}). \quad (5)$$

The relative threshold is the α -th quantile of consecutive differences $\Delta \mathbf{H}^{(c)} = [H(x_t^{(c)}) - H(x_{t-1}^{(c)})]_{t=2}^L$,

$$\gamma_{\text{rel}}^{(c)} = Q_\alpha(\Delta \mathbf{H}^{(c)}), \quad (6)$$

where α is the quantile parameter (e.g., $\alpha = 75\%$). This formulation enables automatic adaptation to varying entropy levels across sequences, eliminating dataset-specific threshold tuning.

Boundary Detection. A patch boundary is placed at position t based on the following conditions:

$$H(x_t^{(c)}) > \theta_{\text{abs}}^{(c)} \quad (\text{high absolute uncertainty}) \quad (7)$$

$$\Delta H(x_t^{(c)}) > \gamma_{\text{rel}}^{(c)} \quad (\text{significant uncertainty increase}) \quad (8)$$

$$M_{t-1}^{(c)} = 0 \quad (\text{no consecutive boundaries}). \quad (9)$$

This threshold mechanism produces a binary patch boundary mask $M^{(c)} \in \{0, 1\}^L$ where $M_t^{(c)} = 1$ indicates a patch start. The framework supports using either threshold independently or in combination, allowing flexible adaptation to different temporal characteristics. EDP outputs mask M for subsequent non-overlapping patch processing.

Patch Segmentation. Given boundary mask $M^{(c)}$, we extract boundary positions $\mathcal{B}^{(c)} = \{t : M_t^{(c)} = 1\} = \{b_1^{(c)}, b_2^{(c)}, \dots, b_{P^{(c)}}^{(c)}\}$ where $b_1^{(c)} = 1$ and $b_{P^{(c)}}^{(c)} = L + 1$. The sequence is then partitioned into $P^{(c)}$ non-overlapping patches:

$$x^{(c)} = \bigcup_{j=1}^{P^{(c)}} p_j^{(c)}, \quad (10)$$

where $p_j^{(c)} = [x_{b_j^{(c)}}, x_{b_j^{(c)}+1}, \dots, x_{b_{j+1}^{(c)}-1}] \in \mathbb{R}^{\ell_j^{(c)}}$, $\ell_j^{(c)} = b_{j+1}^{(c)} - b_j^{(c)}$ is the length of patch j , and $\sum_{j=1}^{P^{(c)}} \ell_j^{(c)} = L$. Our segmentation depends only on relative uncertainty structure, not absolute probability calibration.

3.5. Adaptive Patch Encoder (APE)

The EDP produces variable-length patches where both patch count and individual lengths vary across samples. As shown in Fig. 2(B), the APE converts these heterogeneous patches into fixed-size representations suitable for transformer processing while preserving temporal information. When handling variable patches, we ensure batch processing compatibility by padding sequences to the maximum patch count within each batch and applying attention masks to handle variable patch lengths during cross-attention operations.

Architecture Design. Our encoder employs a two-stage approach. First initial dimensionality reduction via pooling (from time-point embeddings to initial patch embeddings), followed by iterative cross-attention refinement. This design choice is inspired by the Perceiver architecture (Jaegle et al., 2021) and Byte Latent Transformer (Pagnoni et al., 2025), due to their demonstrated performance on language and image data.

Patch Encoding. Each variable-length patch $p_j^{(c)}$ is encoded into a fixed-dimensional representation via the APE. First, we obtain time-point embeddings through an embedding layer $E : \mathcal{V} \rightarrow \mathbb{R}^{d_t}$:

$$\mathbf{h}_t^{(c)} = E(q(x_t^{(c)})), \quad t = 1, \dots, L. \quad (11)$$

For patch $p_j^{(c)}$ spanning positions $\mathcal{T}_j^{(c)} = \{b_j^{(c)}, b_j^{(c)} + 1, \dots, b_{j+1}^{(c)} - 1\}$, we initialize its representation via max pooling:

$$\mathbf{z}_j^{(c),0} = \text{MaxPool} \left(\{\mathbf{h}_t^{(c)}\}_{t \in \mathcal{T}_j^{(c)}} \right) \in \mathbb{R}^{d_p}. \quad (12)$$

We then refine patch embeddings through N cross-attention layers where patch embeddings query only their constituent time points:

$$\mathbf{z}_j^{(c),n} = \mathbf{z}_j^{(c),n-1} + W_o \sum_{i \in \mathcal{T}_j^{(c)}} \alpha_{ji}^{(n)} W_v(\mathbf{h}_i^{(c),n-1}) \quad (13)$$

where attention weights are computed only within the patch:

$$\alpha_{ji}^{(n)} = \frac{\exp \left(\frac{[W_q(\mathbf{z}_j^{(c),n-1})]^\top W_k(\mathbf{h}_i^{(c),n-1})}{\sqrt{d_k}} \right)}{\sum_{i' \in \mathcal{T}_j^{(c)}} \exp \left(\frac{[W_q(\mathbf{z}_j^{(c),n-1})]^\top W_k(\mathbf{h}_{i'}^{(c),n-1})}{\sqrt{d_k}} \right)} \quad (14)$$

This produces final patch embeddings $P^{(c)} = [\mathbf{z}_1^{(c),N}, \dots, \mathbf{z}_{P^{(c)}}^{(c),N}] \in \mathbb{R}^{P^{(c)} \times d_p}$ and encoder hidden states $H^{(c)} = [\mathbf{h}_1^{(c),N}, \dots, \mathbf{h}_L^{(c),N}] \in \mathbb{R}^{L \times d_t}$.

Batch Processing with Variable Patches. For a batch of B samples with varying patch counts $\{P^{(b,c)}\}$, let $P_{\max} = \max_{b,c} P^{(b,c)}$. We construct a padded patch embedding tensor $\tilde{P}^{in} \in \mathbb{R}^{(B \cdot C) \times P_{\max} \times d_p}$ with attention mask $\mathcal{M} \in \{0, 1\}^{(B \cdot C) \times P_{\max}}$ where $\mathcal{M}_{bc,j} = \mathbb{1}[j \leq P^{(b,c)}]$ to mask padded positions during self-attention.

3.6. Global Transformer & Fusion Decoder

The final components of the EntroPE process are the fixed-size patch embeddings to learn long-term dependencies and generate predictions.

Global Transformer. Patch embeddings are processed through a standard transformer to capture inter-patch dependencies:

$$\tilde{P}^{(c)} = \text{Transformer}(P^{(c)}, \mathcal{M}) \in \mathbb{R}^{P^{(c)} \times d_p} \quad (15)$$

Fusion Decoder. We fuse global patch context with fine-grained temporal information via cross-attention where time-point embeddings query patch representations:

$$\begin{aligned} \tilde{H}^{(c)} &= H^{(c)} + \\ &W_o \left(\text{softmax} \left(\frac{[W_q(H^{(c)})][W_k(\tilde{P}^{(c)})]^\top}{\sqrt{d_k}} \right) W_v(\tilde{P}^{(c)}) \right) \\ &\in \mathbb{R}^{L \times d_t} \quad (16) \end{aligned}$$

This mechanism enables knowledge transfer from high-level patch representations back to detailed time-point embeddings, preserving both local temporal patterns and global contextual dependencies.

Task-Specific Head. The enriched representations $\tilde{H}^{(c)}$ are projected to generate future predictions. We apply flattening followed by a linear projection with Instance De-Normalization: $\text{InstanceDeNorm}(W_{\text{proj}}(\text{Flatten}(\tilde{H}^{(c)})))$. Training criteria and additional details on task-specific heads are provided in Appendix B.

4. Experiments

In the section we evaluate the efficacy of EntroPE on long-term forecasting, classification and anomaly detection tasks. We show that our model can serve as a foundation model with competitive performance across these tasks.

4.1. Long-Term Forecasting

Datasets. To examine forecasting performance we conduct comprehensive evaluations on six widely-used long-term multivariate forecasting datasets. i.e., Electricity (ECL) featuring electricity consumption data, ETT family (ETTh1,

ETTh2, ETTm1, ETTm2) that encompass a range of scenarios in energy transfer technology, Weather that offers insights into various meteorological variables over time. Detailed descriptions in Appendix Tab. 6.

Baselines and Experimental Settings. We benchmark against fifteen state-of-the-art baselines. (1) Transformer-based models: TimeMosaic (Ding et al., 2025), iTransformer (Liu et al., 2024b), PatchTST (Nie et al., 2023), FEDformer (Zhou et al., 2022), Autoformer (Wu et al., 2021); (2) CNN-based model: TimesNet (Wu et al., 2023), TSLANet (Eldele et al., 2024); (3) MLP-based models: TimeMixer (Wang et al., 2024), HDMixer (Huang et al., 2024), DLIn-ear (Zeng et al., 2023); (4) Foundation and lightweight models: Time-FFM (Liu et al., 2024a), TimeBase (Huang et al., 2025a); (5) LLM-aligned and cross-modal models: LangTime (Niu et al., 2025), CALF (Liu et al., 2025b); (6) Filter-based model: FilterTS (Wang et al., 2025). (Further details on baselines are discussed in Appendix D.1.)

Results. Table 1 shows EntroPE achieves competitive or superior performance across all baseline categories (Transformer, CNN, MLP, foundation, LLM-aligned, and filter-based models). While retaining PatchTST-like architecture, EntroPE introduces dynamic patching and adaptive encoding, yielding 20% MSE reduction on ETTh1, 15% on Electricity, and 10% average improvement over PatchTST, alongside reduced token count through non-overlapping patches. Notably, iTransformer and CALF demonstrates remarkable performance on high-dimensional Electricity dataset (321 variables) due to its channel-wise attention design. While CALF (~18M parameters) and LangTime (~500M parameters) show competitive results, EntroPE achieves comparable accuracy with 500-1000 \times fewer parameters (100k-1M), demonstrating that entropy-guided segmentation provides robust improvements without requiring massive model capacity.

Compared to some noteworthy dynamic or adaptive patching approaches such as HDMixer and TimeMosaic, EntroPE consistently delivers stronger or more stable gains across datasets. Notably, TimeMosaic employs substantially larger models (3-13M parameters) and higher training durations, whereas EntroPE achieves comparable or better accuracy with smaller models. This highlights that performance gains arise from principled entropy-driven boundary placement rather than increased model capacity. (Full table: Tab. 16 & 17)

4.2. Classification

Datasets. To demonstrate the generalizability of EntroPE beyond forecasting, we evaluate on 10 UEA multivariate time series classification datasets (Bagnall et al., 2018). We replace the forecasting head with a classification head while

Table 1. Multivariate time series forecasting results on benchmark datasets. Results are averaged across prediction horizons $T = \{96, 192, 336, 720\}$ with fixed input length $L = 96$ for all datasets. Best results are highlighted in **red** and second-best in **blue**.

Models	ETTh1		ETTh2		ETTm1		ETTm2		Weather		Electricity	
	MSE	MAE										
Autoformer [2021]	0.496	0.487	0.450	0.459	0.588	0.517	0.327	0.371	0.338	0.382	0.227	0.338
FEDformer [2022]	0.498	0.484	0.437	0.449	0.448	0.452	0.305	0.349	0.309	0.360	0.214	0.327
DLinear [2023]	0.461	0.457	0.563	0.519	0.404	0.408	0.354	0.402	0.265	0.315	0.225	0.319
TimesNet [2023]	0.495	0.450	0.414	0.427	0.400	0.406	0.291	0.333	0.251	0.294	0.193	0.304
PatchTST [2023]	0.516	0.484	0.391	0.411	0.406	0.407	0.290	0.334	0.265	0.285	0.216	0.318
Time-FFM [2024]	0.442	0.434	0.382	0.406	0.399	0.402	0.286	0.332	0.270	0.288	0.216	0.299
HDMixer [2024]	0.448	0.437	0.384	0.407	0.396	0.402	0.286	0.331	0.253	0.285	0.205	0.295
iTransformer [2024]	0.454	0.447	0.383	0.407	0.407	0.410	0.288	0.332	0.258	0.278	0.178	0.270
TimeMixer [2024]	0.459	0.444	0.390	0.409	0.382	0.397	0.279	0.324	0.245	0.276	0.182	0.272
TSLANet [2024]	0.448	0.441	0.372	0.399	0.378	0.397	0.283	0.327	0.259	0.280	0.199	0.283
TimeBase [2025]	0.463	0.429	0.409	0.425	0.431	0.420	0.290	0.332	0.252	0.279	0.227	0.296
LangTime [2025]	0.437	0.425	0.375	0.392	0.397	0.392	0.284	0.321	0.252	0.273	0.201	0.285
FilterTS [2025]	0.440	0.432	0.375	0.399	0.386	0.397	0.279	0.323	0.253	0.280	0.184	0.275
CALF [2025]	0.441	0.435	0.372	0.395	0.396	0.391	0.280	0.321	0.250	0.274	0.177	0.266
TimeMosaic [2026]	0.427	0.442	0.369	0.399	0.388	0.392	0.278	0.319	0.253	0.277	0.188	0.281
EntroPE [2026]	0.416	0.425	0.366	0.387	0.378	0.391	0.286	0.335	0.242	0.273	0.182	0.271

keeping the core architecture unchanged.

Baselines and Experimental Settings. We select eight state-of-the-art baselines, i.e., TSLANet, GPT4TS (Zhou et al., 2023), TimesNet, ROCKET (Dempster et al., 2020), TS-TCC (Eldele et al., 2021), Crossformer (Zhang & Yan, 2023) and PatchTST as they showed the best classification accuracy over other Transformer-based architectures. Last, we experiment with a simple single-layer MLP.

Results. Table 2 shows EntroPE achieves an average accuracy of 77.13%, competitive with TSLANet (76.03%), and outperforming TimesNet (69.36%), PatchTST (71.14%), and other competitive baselines. This demonstrates that entropy-guided dynamic patching effectively captures discriminative temporal patterns for classification tasks.

Anomaly Detection Evaluation. Appendix C shows the detailed information on datasets, baselines and results of EntroPE’s Anomaly detection performance.

4.3. Ablation Study

Model component analysis. To evaluate each component’s contribution, we conduct comprehensive ablation studies across four datasets (ETTh1, ETTh2, ETTm1, Weather) using prediction horizons of 336 and 720, measuring performance via MSE. We progressively remove components from our full EntroPE architecture to create four configurations: (1) EntroPE (Full): Dynamic patching + Adaptive encoder + Fusion decoder; (2) EntroPE - Dynamic: Static patching + Adaptive encoder + Fusion decoder; (3) EntroPE - (Dynamic Patching + Adaptive Encoder): Static patching + Max pooling + Fusion decoder; (4) EntroPE - (Dynamic Patching + Adaptive Encoder + Fusion Decoder): Static patching + Max pooling + Flattened output.

The full EntroPE architecture achieves the best performance across all datasets and horizons, while systematic component removal leads to progressive performance degradation (Table 3). The EntroPE - Dynamic Patching configuration yields second-best results, demonstrating the significant contribution of dynamic boundary detection. Further removing the adaptive encoder (EntroPE - (Dynamic Patching + Adaptive Encoder)) shows additional degradation, validating our cross-attention-based encoder design. The worst performance occurs when all three components are removed, producing only static patching with basic pooling and flattened output. This systematic performance decline confirms that each architectural choice addresses specific modeling challenges in time series forecasting.

Dynamic vs. Static Patching. In addition to the component ablations, we compare EntroPE with dynamic patching against three static (fixed-length, non-overlapping) patching schemes. Experiments are conducted on ETTh1, ETTm1, and Weather datasets with a fixed input length of 96 and forecasting horizons of 336 and 720. Dynamic patching achieves the lowest MSE in most settings (Table 3), while single-token input (patch length of 1) remains competitive, notably without leveraging the Dynamic Patching scheme. However, the computational cost of this setting is substantially higher, as the self-attention mechanism must attend to every time step individually. Figure 3 illustrates the efficiency advantage of dynamic patching over static alternatives under different configurations.

Threshold Sensitivity. We further investigate the effect of the entropy threshold on EntroPE’s performance using the ETTh1 and Weather datasets, which represent small and medium-scale benchmarks. As shown in Figure 4, the MSE values for the 96→336 forecasting setting remain stable across *sample-adaptive* threshold percentile in the range

Table 2. Classification accuracy (%) on 10 UEA multivariate classification datasets.

Dataset	EntroPE [2026]	TSLANet [2024]	GPT4TS [2023]	TimesNet [2023]	ROCKET [2020]	CrossF. [2023]	PatchTST [2023]	MLP [-]	TS-TCC [2021]
EthanolConcentration	29.1	30.42	25.48	27.73	42.58	34.98	28.90	33.46	32.32
FaceDetection	69.1	66.77	65.58	67.47	64.70	66.17	68.96	67.42	63.05
Handwriting	57.4	57.88	34.56	26.18	48.47	26.24	26.00	22.47	47.76
Heartbeat	77.9	77.56	36.59	74.48	69.76	76.59	73.17	77.07	
JapaneseVowels	99.2	99.19	98.11	97.83	95.68	98.92	98.65	97.84	97.30
PEMS-SF	88.6	83.82	87.28	88.13	75.10	82.08	88.44	82.08	86.71
SelfRegulationSCP1	92.9	91.81	91.47	77.43	84.64	92.49	89.76	88.40	91.13
SelfRegulationSCP2	63.1	61.67	51.67	52.84	54.44	53.33	54.44	51.67	53.89
SpokenArabicDigits	99.8	99.91	99.36	98.36	99.20	96.41	99.68	96.68	99.77
UWaveGestureLibrary	94.4	91.25	84.38	83.13	76.03	81.56	80.00	81.88	86.25
Average	77.13	76.03	67.45	69.36	72.90	70.88	71.14	69.51	73.53

Table 3. Component importance and dynamic vs. static patching comparison. Best and second-best are highlighted in red and blue.

Dataset T	Full		-EDP		-EDP		-APE		-EDP		-APE		-FD	
	Dynamic	Static(1)	Static(8)	Static(16)	Pool + FD	Pool	+	FD	Pool	+	FD	Pool	+	FD
ETTh1	336	0.429 0.439	0.425 0.460	0.441	0.444	0.438	0.519							
	720			0.469	0.477	0.461		0.527						
ETTh2	336	0.355 0.397	0.428 0.448	0.435	0.439	0.439	0.462							
	720			0.470	0.463	0.466		0.456						
ETTm1	336	0.393 0.445	0.401 0.451	0.409	0.415	0.402	0.427							
	720			0.459	0.452	0.457		0.483						
Weather	336	0.258 0.341	0.261 0.343	0.265	0.270	0.262	0.262							
	720			0.353	0.359	0.347		0.346						

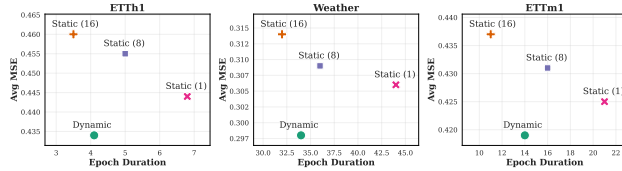


Figure 3. Dynamic and Static(patch_length) patching with epoch duration.

15%-95%, indicating robustness to threshold selection. At the same time, training time and patch construction reveal that the threshold effectively acts as a control knob for computational complexity: lower thresholds yield more patches (higher cost), while higher thresholds reduce the number of patches and speed up (31% in Weather and 25% in ETTh1) training, with minimal variation in predictive accuracy.

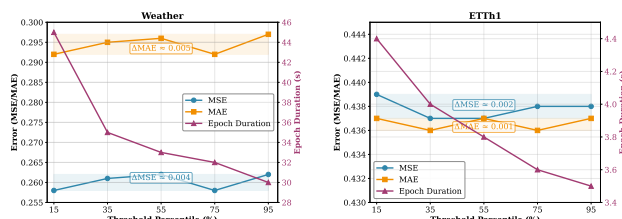


Figure 4. Threshold sensitivity with epoch duration.

4.4. Efficiency Analysis

As shown in Figures 3 and 4, our model adapts to different patching schemes, directly affecting computational efficiency. We evaluate efficiency on the ETTh1 dataset (96→96) by comparing recent models in terms of Multiply-Accumulate Operations (MACs), MSE, and the number of trainable parameters. Figure 5 demonstrates that our model achieves a more favorable performance-efficiency trade-off, with bubble size proportional to the parameter count. Notably, while TimeMixer and TimeKAN (Huang et al., 2025b) occupy a nearby region in the trade-off space, our model attains a superior position, especially with its transformer-based architecture. (See full table: Tab. 13)

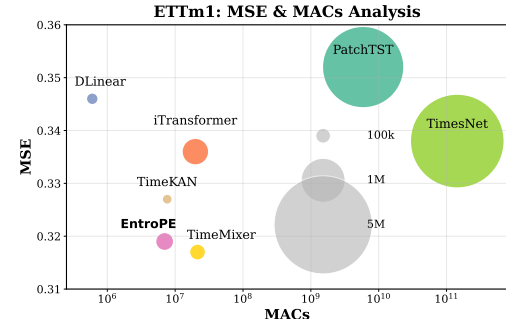


Figure 5. EntroPE's efficiency analysis on ETTh1 dataset.

5. Conclusion

We introduced EntroPE, a dynamic patch encoding framework that uses entropy-guided boundary detection to identify natural temporal transitions in time series. By placing patch boundaries at information-rich transitions rather than fixed intervals, EntroPE preserves temporal coherence while enabling efficient variable-length processing. This information-theoretic approach improves performance across downstream tasks with practical computational benefits. Beyond empirical gains, EntroPE demonstrates the value of respecting intrinsic temporal structure, opening new directions in adaptive context-aware sequence modeling.

Impact Statement

This paper presents work whose goal is to advance the field of Machine Learning. There are many potential societal consequences of our work, none which we feel must be specifically highlighted here.

References

Abdulaal, A., Liu, Z., and Lancewicki, T. Practical approach to asynchronous multivariate time series anomaly detection and localization. In *Proceedings of the 27th ACM SIGKDD conference on knowledge discovery & data mining*, pp. 2485–2494, 2021.

Ansari, A. F., Stella, L., Turkmen, C., Zhang, X., Mercado, P., Shen, H., Shchur, O., Rangapuram, S. S., Arango, S. P., Kapoor, S., Zschiegner, J., Maddix, D. C., Mahoney, M. W., Torkkola, K., Wilson, A. G., Bohlke-Schneider, M., and Wang, Y. Chronos: Learning the language of time series. *Transactions on Machine Learning Research*, 2024. ISSN 2835-8856. URL <https://openreview.net/forum?id=gerNCVqqtR>.

Bagnall, A., Dau, H. A., Lines, J., Flynn, M., Large, J., Bostrom, A., Southam, P., and Keogh, E. The uea multivariate time series classification archive, 2018. *arXiv preprint arXiv:1811.00075*, 2018.

Cao, Y., Tian, Z., Guo, W., and Liu, X. Mspatch: A multi-scale patch mixing framework for multivariate time series forecasting. *Expert Syst. Appl.*, 273:126849, 2025. URL <https://doi.org/10.1016/j.eswa.2025.126849>.

Chen, P., Zhang, Y., Cheng, Y., Shu, Y., Wang, Y., Wen, Q., Yang, B., and Guo, C. Pathformer: Multi-scale transformers with adaptive pathways for time series forecasting. In *International Conference on Learning Representations (ICLR)*, 2024.

Cirstea, R.-G., Guo, C., Yang, B., Kieu, T., Dong, X., and Pan, S. Triformer: Triangular, variable-specific attentions for long sequence multivariate time series forecasting. In Raedt, L. D. (ed.), *Proceedings of the Thirty-First International Joint Conference on Artificial Intelligence, IJCAI-22*, pp. 1994–2001. International Joint Conferences on Artificial Intelligence Organization, 7 2022. doi: 10.24963/ijcai.2022/277. URL <https://doi.org/10.24963/ijcai.2022/277>. Main Track.

Das, A., Kong, W., Sen, R., and Zhou, Y. A decoder-only foundation model for time-series forecasting. In *Forty-first International Conference on Machine Learning*, 2024.

Dempster, A., Petitjean, F., and Webb, G. I. Rocket: exceptionally fast and accurate time series classification using random convolutional kernels. *Data Mining and Knowledge Discovery*, 34(5):1454–1495, 2020.

Ding, K., Fan, F., Hou, C., Wang, Z., Wang, L., Yang, Z., and Zhan, J. Timemosaic: Temporal heterogeneity guided time series forecasting via adaptive granularity patch and segment-wise decoding. *arXiv preprint arXiv:2509.19406*, 2025.

Dosovitskiy, A., Beyer, L., Kolesnikov, A., Weissenborn, D., Zhai, X., Unterthiner, T., Dehghani, M., Minderer, M., Heigold, G., Gelly, S., Uszkoreit, J., and Houlsby, N. An image is worth 16x16 words: Transformers for image recognition at scale. In *International Conference on Learning Representations*, 2021. URL <https://openreview.net/forum?id=YicbFdNTTy>.

Eldele, E., Ragab, M., Chen, Z., Wu, M., Kwoh, C. K., Li, X., and Guan, C. Time-series representation learning via temporal and contextual contrasting. In *Proceedings of the Thirtieth International Joint Conference on Artificial Intelligence, IJCAI-21*, pp. 2352–2359, 2021.

Eldele, E., Ragab, M., Chen, Z., Wu, M., and Li, X. Tslanet: Rethinking transformers for time series representation learning. In *International Conference on Machine Learning*, 2024.

Fischer, T. and Krauss, C. Deep learning with long short-term memory networks for financial market predictions. *European journal of operational research*, 270(2):654–669, 2018.

Gasparin, A., Lukovic, S., and Alippi, C. Deep learning for time series forecasting: The electric load case. *CAAI Transactions on Intelligence Technology*, 7(1):1–25, 2022.

Huang, Q., Shen, L., Zhang, R., Cheng, J., Ding, S., Zhou, Z., and Wang, Y. Hdmixer: Hierarchical dependency with extendable patch for multivariate time series forecasting. In *Proceedings of the AAAI conference on artificial intelligence*, pp. 12608–12616, 2024.

Huang, Q., Zhou, Z., Yang, K., Yi, Z., Wang, X., and Wang, Y. Timebase: The power of minimalism in efficient long-term time series forecasting. In *Forty-second International Conference on Machine Learning*, 2025a.

Huang, S., Zhao, Z., Li, C., and BAI, L. TimeKAN: KAN-based frequency decomposition learning architecture for long-term time series forecasting. In *The Thirteenth International Conference on Learning Representations*, 2025b. URL <https://openreview.net/forum?id=wTlc79YNbh>.

Hundman, K., Constantinou, V., Laporte, C., Colwell, I., and Soderstrom, T. Detecting spacecraft anomalies using lstms and nonparametric dynamic thresholding. In *Proceedings of the 24th ACM SIGKDD international conference on knowledge discovery & data mining*, pp. 387–395, 2018.

Jaegle, A., Gimeno, F., Brock, A., Vinyals, O., Zisserman, A., and Carreira, J. Perceiver: General perception with iterative attention. In *International conference on machine learning*, pp. 4651–4664. PMLR, 2021.

Lee, S., Park, T., and Lee, K. Learning to embed time series patches independently. In *The Twelfth International Conference on Learning Representations*, 2024. URL <https://openreview.net/forum?id=WS7GuBDFa2>.

Lim, B. and Zohren, S. Time-series forecasting with deep learning: a survey. *Philosophical Transactions of the Royal Society A*, 379(2194):20200209, 2021.

Liu, K., Duan, Z., Chen, C., Wang, Y., Cheng, D., and Liang, Y. Adapatch: Adaptive patch-level modeling for non-stationary time series forecasting. In *Proceedings of the 34th ACM International Conference on Information and Knowledge Management*, pp. 1882–1891, 2025a.

Liu, P., Guo, H., Dai, T., Li, N., Bao, J., Ren, X., Jiang, Y., and Xia, S.-T. Calf: Aligning llms for time series forecasting via cross-modal fine-tuning. *Proceedings of the AAAI Conference on Artificial Intelligence*, 39(18):18915–18923, Apr. 2025b. doi: 10.1609/aaai.v39i18.34082. URL <https://ojs.aaai.org/index.php/AAAI/article/view/34082>.

Liu, Q., Liu, X., Liu, C., Wen, Q., and Liang, Y. Time-ffm: Towards lm-empowered federated foundation model for time series forecasting. *Advances in Neural Information Processing Systems*, 37:94512–94538, 2024a.

Liu, X., Qiu, X., Wu, X., Li, Z., Guo, C., Hu, J., and Yang, B. Rethinking irregular time series forecasting: A simple yet effective baseline. *arXiv preprint arXiv:2505.11250*, 2025c.

Liu, Y., Hu, T., Zhang, H., Wu, H., Wang, S., Ma, L., and Long, M. itransformer: Inverted transformers are effective for time series forecasting. In *The Twelfth International Conference on Learning Representations*, 2024b. URL <https://openreview.net/forum?id=JePfAI8fah>.

Mathur, A. P. and Tippenhauer, N. O. Swat: A water treatment testbed for research and training on ics security. In *2016 international workshop on cyber-physical systems for smart water networks (CySWater)*, pp. 31–36. IEEE, 2016.

Nie, Y., H. Nguyen, N., Sinthong, P., and Kalagnanam, J. A time series is worth 64 words: Long-term forecasting with transformers. In *International Conference on Learning Representations*, 2023.

Niu, W., Xie, Z., Sun, Y., He, W., Xu, M., and Hao, C. Lang-time: A language-guided unified model for time series forecasting with proximal policy optimization. In *Forty-second International Conference on Machine Learning*, 2025. URL <https://openreview.net/forum?id=VfoKOD65Zq>.

Pagnoni, A., Pasunuru, R., Rodriguez, P., Nguyen, J., Muller, B., Li, M., Zhou, C., Yu, L., Weston, J. E., Zettlemoyer, L., et al. Byte latent transformer: Patches scale better than tokens. In *Proceedings of the 63rd Annual Meeting of the Association for Computational Linguistics (Volume 1: Long Papers)*, pp. 9238–9258, 2025.

Radford, A., Wu, J., Child, R., Luan, D., Amodei, D., Sutskever, I., et al. Language models are unsupervised multitask learners. *OpenAI blog*, 1(8):9, 2019.

Reis, B. Y. and Mandl, K. D. Time series modeling for syndromic surveillance. *BMC medical informatics and decision making*, 3(1):2, 2003.

Smith, R. L. Extreme value analysis of environmental time series: an application to trend detection in ground-level ozone. *Statistical Science*, pp. 367–377, 1989.

Stitsyuk, A. and Choi, J. xpatch: Dual-stream time series forecasting with exponential seasonal-trend decomposition. In *Proceedings of the AAAI Conference on Artificial Intelligence*, pp. 20601–20609, 2025.

Su, Y., Zhao, Y., Niu, C., Liu, R., Sun, W., and Pei, D. Robust anomaly detection for multivariate time series through stochastic recurrent neural network. In *Proceedings of the 25th ACM SIGKDD international conference on knowledge discovery & data mining*, pp. 2828–2837, 2019.

Tang, P. and Zhang, W. Unlocking the power of patch: Patch-based mlp for long-term time series forecasting. In *Proceedings of the AAAI Conference on Artificial Intelligence*, pp. 12640–12648, 2025.

Torres, J. F., Hadjout, D., Sebaa, A., Martínez-Álvarez, F., and Troncoso, A. Deep learning for time series forecasting: a survey. *Big data*, 9(1):3–21, 2021.

Vaswani, A., Shazeer, N., Parmar, N., Uszkoreit, J., Jones, L., Gomez, A. N., Kaiser, Ł., and Polosukhin, I. Attention is all you need. *Advances in neural information processing systems*, 30, 2017.

Wang, S., Wu, H., Shi, X., Hu, T., Luo, H., Ma, L., Zhang, J. Y., and ZHOU, J. Timemixer: Decomposable multi-scale mixing for time series forecasting. In *International Conference on Learning Representations (ICLR)*, 2024.

Wang, Y., Liu, Y., Duan, X., and Wang, K. Filters: Comprehensive frequency filtering for multivariate time series forecasting. *Proceedings of the AAAI Conference on Artificial Intelligence*, 39(20): 21375–21383, Apr. 2025. doi: 10.1609/aaai.v39i20.35438. URL <https://ojs.aaai.org/index.php/AAAI/article/view/35438>.

Wen, Q., Zhou, T., Zhang, C., Chen, W., Ma, Z., Yan, J., and Sun, L. Transformers in time series: A survey. In *International Joint Conference on Artificial Intelligence(IJCAI)*, 2023.

Woo, G., Liu, C., Sahoo, D., Kumar, A., and Hoi, S. Ets-former: Exponential smoothing transformers for time-series forecasting. *arXiv preprint arXiv:2202.01381*, 2022.

Woo, G., Liu, C., Kumar, A., Xiong, C., Savarese, S., and Sahoo, D. Unified training of universal time series forecasting transformers. In *Forty-first International Conference on Machine Learning*, 2024. URL <https://openreview.net/forum?id=Yd8eHMY1wz>.

Wu, H., Xu, J., Wang, J., and Long, M. Autoformer: Decomposition transformers with auto-correlation for long-term series forecasting. *Advances in neural information processing systems*, 34:22419–22430, 2021.

Wu, H., Hu, T., Liu, Y., Zhou, H., Wang, J., and Long, M. Timesnet: Temporal 2d-variation modeling for general time series analysis. In *International Conference on Learning Representations*, 2023.

Wu, X., Qiu, X., Cheng, H., Li, Z., Hu, J., Guo, C., and Yang, B. Enhancing time series forecasting through selective representation spaces: A patch perspective. In *The Thirty-ninth Annual Conference on Neural Information Processing Systems*, 2025.

Xue, W., Zhou, T., Wen, Q., Gao, J., Ding, B., and Jin, R. Card: Channel aligned robust blend transformer for time series forecasting. In *International Conference on Learning Representations (ICLR)*, 2024.

Zeng, A., Chen, M., Zhang, L., and Xu, Q. Are transformers effective for time series forecasting? In *Proceedings of the AAAI conference on artificial intelligence*, pp. 11121–11128, 2023.

Zhang, Y. and Yan, J. Crossformer: Transformer utilizing cross-dimension dependency for multivariate time series forecasting. In *The eleventh international conference on learning representations*, 2023.

Zhang, Y., Zhou, K., and Liu, Z. Neural prompt search. *IEEE Transactions on Pattern Analysis and Machine Intelligence*, 2024.

Zhou, H., Zhang, S., Peng, J., Zhang, S., Li, J., Xiong, H., and Zhang, W. Informer: Beyond efficient transformer for long sequence time-series forecasting. In *Proceedings of the AAAI conference on artificial intelligence*, pp. 11106–11115, 2021.

Zhou, T., Ma, Z., Wen, Q., Wang, X., Sun, L., and Jin, R. Fedformer: Frequency enhanced decomposed transformer for long-term series forecasting. In *International conference on machine learning*, pp. 27268–27286. PMLR, 2022.

Zhou, T., Niu, P., Sun, L., Jin, R., et al. One fits all: Power general time series analysis by pretrained lm. *Advances in neural information processing systems*, 36:43322–43355, 2023.

A. Preliminaries & Motivation

A.1. Method Overview

Our approach consists of two distinct phases: (1) *entropy model pre-training* for uncertainty quantification, and (2) *task-specific training* with entropy-guided dynamic patching. Crucially, the entropy model parameters remain frozen during task-specific training, serving solely to provide patch boundaries.

A.2. Theoretical Motivation

We provide a theoretical justification for entropy-guided patch segmentation. Our framework rests on two principles: (i) conditional entropy characterizes irreducible predictive uncertainty, and (ii) segmenting sequences at high-entropy points yields patches with lower intra-segment uncertainty and improved temporal coherence.

Proposition A.1 (Conditional Entropy Lower-Bounds Irreducible Prediction Loss). *Let $\tau_{1:L}$ denote quantized time-series tokens and let $p_*(\tau_{t+1} | \tau_{\leq t})$ be the true next-token conditional distribution. For any predictive model $q(\tau_{t+1} | \tau_{\leq t})$, the expected one-step negative log-likelihood satisfies*

$$\mathbb{E}_{p_*}[-\log q(\tau_{t+1} | \tau_{\leq t})] \geq H_*(\tau_{t+1} | \tau_{\leq t}), \quad (17)$$

with equality if and only if $q(\cdot | \tau_{\leq t}) = p_*(\cdot | \tau_{\leq t})$ almost surely.

Proof sketch. By the cross-entropy decomposition,

$$\mathbb{E}_{p_*}[-\log q] = H_*(\tau_{t+1} | \tau_{\leq t}) + \text{KL}(p_*(\cdot | \tau_{\leq t}) \| q(\cdot | \tau_{\leq t})),$$

and since $\text{KL}(\cdot \| \cdot) \geq 0$, the bound follows, with equality if and only if $q = p_*$ almost surely. \square

Proposition A.2 (High-Entropy Boundaries Reduce Intra-Patch Predictive Uncertainty). *Let a segmentation $\mathcal{S} = \{1 = b_1 < b_2 < \dots < b_{P+1} = L+1\}$ partition a sequence into patches $[b_j, b_{j+1})$. Define the total within-patch uncertainty mass as*

$$U(\mathcal{S}) = \sum_{j=1}^P \sum_{t=b_j}^{b_{j+1}-1} H_*(\tau_{t+1} | \tau_{\leq t}). \quad (18)$$

Consider a candidate boundary b within a patch $[s, e)$, and suppose $H_(\tau_{b+1} | \tau_{\leq b})$ is a local maximum or exhibits a sharp positive increment relative to its neighborhood. Then introducing a boundary at b yields a segmentation \mathcal{S}' such that the average within-patch entropy*

$$\frac{1}{|[b_j, b_{j+1})|} \sum_{t=b_j}^{b_{j+1}-1} H_*(\tau_{t+1} | \tau_{\leq t})$$

is no greater in at least one resulting patch and strictly lower whenever H_ exhibits a concentrated spike at b .*

Proof sketch. Let $[s, e)$ contain $b \in (s, e)$. Splitting into $[s, b)$ and $[b, e)$ preserves total uncertainty mass, but redistributes it across two segments. If $H_*(\tau_{b+1} | \tau_{\leq b})$ is locally elevated, then keeping b interior inflates the mean uncertainty of the full segment. By relocating b to a boundary, the high-entropy region is isolated to the segment edge, lowering the average entropy within at least one subsegment. This reduces expected intra-patch predictive uncertainty while preserving segmentation budget. \square

Connection to EntroPE. Proposition A.1 establishes conditional entropy as a fundamental lower bound on achievable predictive loss, implying that peaks in entropy correspond to irreducible uncertainty in temporal evolution. Proposition A.2 further motivates entropy-guided segmentation by showing that placing boundaries at high-entropy or sharply rising entropy points yields patches whose interiors exhibit lower average predictive uncertainty and greater temporal coherence.

EntroPE operationalizes this principle by training a lightweight causal transformer on quantized time series, freezing it, and computing per-timestep conditional entropy from the predicted token distribution. Since the true entropy H_* is unknown, we approximate it using the frozen model's predictive distribution, $H_t \approx H_*(\tau_{t+1} | \tau_{\leq t})$, and apply quantile-based thresholding (Eq. 5–6) to construct a boundary mask for dynamic patching. Our segmentation depends only on relative uncertainty structure, not absolute probability calibration.

Remark A.3 (Quantization Does Not Limit Predictions). While we use quantization for entropy computation, the downstream prediction heads operate on continuous representations (Sec. 3.6). This decoupling eliminates range constraints: predictions are not limited to the discrete vocabulary \mathcal{V} used for boundary detection.

This theoretical framework justifies our design: EntroPE identifies natural transition points where predictive uncertainty is high, ensuring patches are internally coherent while boundaries mark regime changes.

A.2.1. PHASE I: ENTROPY MODEL PRE-TRAINING

Given a time series dataset $\mathcal{D}_{\text{pretrain}} = \{X^{(i)}\}_{i=1}^N$ where $X^{(i)} \in \mathbb{R}^{C \times L}$, we first quantize each continuous sequence into discrete tokens. For a univariate sequence $x = [x_1, \dots, x_L]$, we apply quantization $q : \mathbb{R} \rightarrow \mathcal{V}$ (defined in Eq. 38) to obtain tokenized sequence $\tau = [\tau_1, \dots, \tau_L]$ where $\tau_t = q(x_t) \in \mathcal{V}$ and $|\mathcal{V}| = V$.

Automatic Quantization Range. To avoid manual threshold selection, we determine bin boundaries $\{b_1, \dots, b_{V-1}\}$ from training data statistics. Let X_{train} denote z-score normalized training values. We compute empirical quantiles:

$$q_{\text{low}} = Q_{\epsilon/2}(X_{\text{train}}), \quad q_{\text{high}} = Q_{1-\epsilon/2}(X_{\text{train}}) \quad (19)$$

where $\epsilon = 0.005$ captures 99.5% of the distribution. The symmetric quantization radius is $R = \max(|q_{\text{low}}|, |q_{\text{high}}|)$, and the interval $[-R, R]$ is uniformly divided into V bins.

Model Training. We train a lightweight causal transformer $f_{\theta_{\text{ent}}} : \mathcal{V}^t \rightarrow \Delta^V$ (where Δ^V denotes the probability simplex over vocabulary \mathcal{V}) to perform next-token prediction. The model is optimized via:

$$\theta_{\text{ent}}^* = \arg \min_{\theta_{\text{ent}}} \mathbb{E}_{X \sim \mathcal{D}_{\text{pretrain}}} [\mathcal{L}_{\text{CE}}(X; \theta_{\text{ent}})] \quad (20)$$

where the cross-entropy loss for a sequence is:

$$\mathcal{L}_{\text{CE}}(X; \theta_{\text{ent}}) = -\frac{1}{L-1} \sum_{t=1}^{L-1} \log p_{\theta_{\text{ent}}}(\tau_{t+1} | \tau_{\leq t}) \quad (21)$$

Once converged, we freeze θ_{ent}^* and use it exclusively for entropy computation, *not* for prediction or token generation. This decoupling is critical: the entropy model learns predictive uncertainty patterns, while downstream task models operate on continuous representations.

A.2.2. PHASE II: ENTROPY-GUIDED DYNAMIC SEGMENTATION

Entropy Computation. For a new input sequence $X \in \mathbb{R}^{C \times L}$, we process each channel independently. For channel c , we compute the quantized sequence $\tau^{(c)} = [q(x_1^{(c)}), \dots, q(x_L^{(c)})]$ and use the frozen model θ_{ent}^* to calculate conditional entropy at each position:

$$H(x_t^{(c)}; \theta_{\text{ent}}^*) = - \sum_{v \in \mathcal{V}} p_{\theta_{\text{ent}}^*}(\tau_{t+1}^{(c)} = v | \tau_{\leq t}^{(c)}) \log p_{\theta_{\text{ent}}^*}(\tau_{t+1}^{(c)} = v | \tau_{\leq t}^{(c)}) \quad (22)$$

yielding entropy sequence $\mathbf{H}^{(c)} = [H(x_1^{(c)}), \dots, H(x_L^{(c)})] \in \mathbb{R}^L$.

Theoretical Motivation. High conditional entropy $H(x_t | x_{<t})$ indicates temporal transitions where x_t is less predictable from history. By placing boundaries at high-uncertainty regions, patches become internally coherent (low intra-patch entropy) while boundaries mark regime changes. Unlike fixed-length patching, our proposed method doesn't ignore predictive structure.

Adaptive Threshold Determination. Rather than fixed thresholds requiring dataset-specific tuning in general, we introduce sample-adaptive thresholds via quantile estimation. For the α -th quantile (e.g., $\alpha = 0.75$), we derive:

$$\theta_{\text{abs}}^{(c)} = Q_{\alpha}(\mathbf{H}^{(c)}) \quad (\text{absolute entropy threshold}) \quad (23)$$

$$\Delta \mathbf{H}^{(c)} = [H(x_t^{(c)}) - H(x_{t-1}^{(c)})]_{t=2}^L \quad (\text{entropy differences}) \quad (24)$$

$$\gamma_{\text{rel}}^{(c)} = Q_{\alpha}(\Delta \mathbf{H}^{(c)}) \quad (\text{relative entropy threshold}) \quad (25)$$

Boundary Detection. We generate a binary boundary mask $M^{(c)} \in \{0, 1\}^L$ where $M_t^{(c)} = 1$ indicates a patch boundary at position t . Position t becomes a boundary when:

$$M_t^{(c)} = \mathbb{1} \left[H(x_t^{(c)}) > \theta_{\text{abs}}^{(c)} \wedge \Delta H(x_t^{(c)}) > \gamma_{\text{rel}}^{(c)} \wedge M_{t-1}^{(c)} = 0 \right] \quad (26)$$

with $M_1^{(c)} = 1$ (first position always starts a patch).

Patch Segmentation. Given boundary mask $M^{(c)}$, we extract boundary positions $\mathcal{B}^{(c)} = \{t : M_t^{(c)} = 1\} = \{b_1^{(c)}, b_2^{(c)}, \dots, b_{P^{(c)}}^{(c)} + 1\}$ where $b_1^{(c)} = 1$ and $b_{P^{(c)}}^{(c)} + 1 = L + 1$. The sequence is then partitioned into $P^{(c)}$ non-overlapping patches:

$$x^{(c)} = \bigcup_{j=1}^{P^{(c)}} p_j^{(c)}, \quad p_j^{(c)} = [x_{b_j^{(c)}}, x_{b_j^{(c)}+1}, \dots, x_{b_{j+1}^{(c)}-1}] \in \mathbb{R}^{\ell_j^{(c)}} \quad (27)$$

where $\ell_j^{(c)} = b_{j+1}^{(c)} - b_j^{(c)}$ is the length of patch j , and $\sum_{j=1}^{P^{(c)}} \ell_j^{(c)} = L$.

A.2.3. PHASE III: TASK-SPECIFIC TRAINING WITH FIXED BOUNDARIES

Patch Encoding. Each variable-length patch $p_j^{(c)}$ is encoded into a fixed-dimensional representation via the Adaptive Patch Encoder (APE). First, we obtain time-point embeddings through an embedding layer $E : \mathcal{V} \rightarrow \mathbb{R}^{d_t}$:

$$\mathbf{h}_t^{(c)} = E(q(x_t^{(c)})), \quad t = 1, \dots, L \quad (28)$$

For patch $p_j^{(c)}$ spanning positions $\mathcal{T}_j^{(c)} = \{b_j^{(c)}, b_j^{(c)} + 1, \dots, b_{j+1}^{(c)} - 1\}$, we initialize its representation via max pooling:

$$\mathbf{z}_j^{(c),0} = \text{MaxPool} \left(\{\mathbf{h}_t^{(c)}\}_{t \in \mathcal{T}_j^{(c)}} \right) \in \mathbb{R}^{d_p} \quad (29)$$

We then refine patch embeddings through N cross-attention layers where patch embeddings query only their constituent time points:

$$\mathbf{z}_j^{(c),n} = \mathbf{z}_j^{(c),n-1} + W_o \sum_{i \in \mathcal{T}_j^{(c)}} \alpha_{ji}^{(n)} W_v(\mathbf{h}_i^{(c),n-1}) \quad (30)$$

where attention weights are computed only within the patch:

$$\alpha_{ji}^{(n)} = \frac{\exp \left(\frac{[W_q(\mathbf{z}_j^{(c),n-1})]^\top W_k(\mathbf{h}_i^{(c),n-1})}{\sqrt{d_k}} \right)}{\sum_{i' \in \mathcal{T}_j^{(c)}} \exp \left(\frac{[W_q(\mathbf{z}_j^{(c),n-1})]^\top W_k(\mathbf{h}_{i'}^{(c),n-1})}{\sqrt{d_k}} \right)} \quad (31)$$

This produces final patch embeddings $P^{(c)} = [\mathbf{z}_1^{(c),N}, \dots, \mathbf{z}_{P^{(c)}}^{(c),N}] \in \mathbb{R}^{P^{(c)} \times d_p}$ and encoder hidden states $H^{(c)} = [\mathbf{h}_1^{(c),N}, \dots, \mathbf{h}_L^{(c),N}] \in \mathbb{R}^{L \times d_t}$.

Batch Processing with Variable Patches. For a batch of B samples with varying patch counts $\{P^{(b,c)}\}$, let $P_{\max} = \max_{b,c} P^{(b,c)}$. We construct a padded patch embedding tensor $\tilde{P}^{in} \in \mathbb{R}^{(B \cdot C) \times P_{\max} \times d_p}$ with attention mask $\mathcal{M} \in \{0, 1\}^{(B \cdot C) \times P_{\max}}$ where $\mathcal{M}_{bc,j} = \mathbb{1}[j \leq P^{(b,c)}]$ to mask padded positions during self-attention.

Global Transformer. Patch embeddings are processed through a standard transformer to capture inter-patch dependencies:

$$\tilde{P}^{(c)} = \text{Transformer}(P^{(c)}, \mathcal{M}) \in \mathbb{R}^{P^{(c)} \times d_p} \quad (32)$$

Fusion Decoder. We fuse global patch context with fine-grained temporal information via cross-attention where time-point embeddings query patch representations:

$$\tilde{H}^{(c)} = H^{(c)} + W_o \left(\text{softmax} \left(\frac{[W_q(H^{(c)})][W_k(\tilde{P}^{(c)})]^\top}{\sqrt{d_k}} \right) W_v(\tilde{P}^{(c)}) \right) \in \mathbb{R}^{L \times d_t} \quad (33)$$

This mechanism enables knowledge transfer from high-level patch representations back to detailed time-point embeddings, preserving both local temporal patterns and global contextual dependencies.

B. Task-Specific Linear Projection

Task-Specific Heads. The enriched representations are projected to task-specific outputs:

Forecasting: Channel-wise linear projection

$$\hat{Y}^{(c)} = g_{\text{fc}} \left(\text{Flatten}(\tilde{H}^{(c)}) \right) \in \mathbb{R}^T, \quad c = 1, \dots, C \quad (34)$$

with MSE loss: $\mathcal{L}_{\text{forecast}} = \frac{1}{C \cdot T} \sum_{c=1}^C \sum_{t=1}^T (Y_{c,t}^{(c)} - \hat{Y}_{c,t}^{(c)})^2$

Classification: Flatten all channels and project to class logits

$$\hat{y} = g_{\text{cls}} \left(\text{Flatten}([\tilde{H}^{(1)}, \dots, \tilde{H}^{(C)}]) \right) \in \mathbb{R}^K \quad (35)$$

with cross-entropy loss: $\mathcal{L}_{\text{class}} = -\log \frac{\exp(\hat{y}_y)}{\sum_{k=1}^K \exp(\hat{y}_k)}$ where $y \in \{1, \dots, K\}$ is the true label.

Anomaly Detection: Channel-wise reconstruction

$$\hat{X}^{(c)} = g_{\text{rec}} \left(\text{Flatten}(\tilde{H}^{(c)}) \right) \in \mathbb{R}^L, \quad c = 1, \dots, C \quad (36)$$

with MSE loss: $\mathcal{L}_{\text{anomaly}} = \frac{1}{C \cdot L} \sum_{c=1}^C \sum_{t=1}^L (X_{c,t}^{(c)} - \hat{X}_{c,t}^{(c)})^2$

Training Protocol. During task-specific training, the entropy model θ_{ent}^* remains frozen and is used only to compute patch boundaries via Eq. (8)-(10). Only the encoder E , APE, transformer, fusion decoder, and task head parameters $\Phi = \{E, \theta_{\text{APE}}, \theta_{\text{trans}}, \theta_{\text{FD}}, \theta_{\text{task}}\}$ are optimized:

$$\Phi^* = \arg \min_{\Phi} \mathbb{E}_{(X, Y) \sim \mathcal{D}_{\text{task}}} [\mathcal{L}_{\text{task}}(X, Y; \Phi \mid \theta_{\text{ent}}^*)] \quad (37)$$

where $\mathcal{D}_{\text{task}}$ is the task-specific dataset and $\mathcal{L}_{\text{task}} \in \{\mathcal{L}_{\text{forecast}}, \mathcal{L}_{\text{class}}, \mathcal{L}_{\text{anomaly}}\}$.

Computational Complexity. Let L be sequence length, P the average number of patches, and d the hidden dimension. EntroPE's complexity is $\mathcal{O}(Ld + P^2d)$ where $P \ll L$, compared to $\mathcal{O}(L^2d)$ for point-wise models. The entropy threshold α provides explicit control: lower $\alpha \rightarrow$ more boundaries \rightarrow higher $P \rightarrow$ more computation but finer granularity.

C. Anomaly Detection

Datasets. We further evaluate EntroPE on five standard anomaly detection benchmarks (SMD (Su et al., 2019), MSL (Hundman et al., 2018), SMAP (Hundman et al., 2018), SWaT (Mathur & Tippenhauer, 2016), PSM (Abdulaal et al., 2021)) by replacing the forecasting head with an anomaly scoring mechanism. Table 4 shows F1 scores compared to recent methods.

D. Baselines

Baselines and Experimental Settings. Baselines and Experimental Settings. We followed the same experimental settings and adopted the same baselines in TSLANet. These are TSLANet, GPT4TS, TimesNet, PatchTST, ETSformer (Woo et al., 2022), FEDformer, LightTS (Zhang et al., 2024), DLlinear.

Table 4. Anomaly detection F1 scores (%) on benchmark datasets.

Dataset	EntroPE	TSLANet	GPT4TS	TimesNet	PatchTST	ETSformer	FEDformer	LightTS	DLinear
SMD	87.1	87.91	86.89	84.61	84.62	83.13	85.08	82.53	77.10
MSL	85.3	83.32	82.45	81.84	78.70	85.03	78.57	78.95	84.88
SMAP	74.2	75.96	72.88	69.39	68.82	69.50	70.76	69.21	69.26
SWaT	94.3	92.80	94.23	93.02	85.72	84.91	93.19	93.33	87.52
PSM	97.7	97.73	97.13	97.34	96.08	91.76	97.23	97.15	93.55
Average	87.72	87.54	86.72	85.24	82.79	82.87	84.97	84.23	82.46

Results. EntroPE attains an average F1 score of 87.72%, competitive with or better than TSLANet (87.54%), GPT4TS (86.72%), TimesNet (85.24%), and other baselines. These results confirm that the entropy-guided patching mechanism generalizes beyond forecasting to anomaly detection tasks.

D.1. Baseline Details

See Table 5 for the details about each baseline.

Table 5. Overview of baseline models (2021–2025) grouped by architecture. We highlight their key design paradigms for deep time series forecasting.

Model	Category	Key Features / Innovations
TimeMosaic (Ding et al., 2025)	Transformer	patch granularity based on temporal heterogeneity and motif reuse.
iTransformer (Liu et al., 2024b)	Transformer	Inverted attention across feature and time dimensions.
PatchTST (Nie et al., 2023)	Transformer	Patch-based embedding with channel-independence.
FEDformer (Zhou et al., 2022)	Transformer (freq.-decomp.)	Fourier/Wavelet enhanced decomposition.
Autoformer (Wu et al., 2021)	Transformer (decomp.-autocorr.)	Progressive decomposition with auto-correlation.
TimesNet (Wu et al., 2023)	CNN	Temporal 2D variation modeling with convolutional layers.
TSLANet (Eldele et al., 2024)	CNN + Lightweight	Lightweight and pretraining module for enhanced feature representation
TimeMixer (Wang et al., 2024)	MLP	Multiscale mixing, separation of trend and seasonal signals.
HDMixer (Huang et al., 2024)	MLP	Hierarchical dependency with extendable patches.
DLinear (Zeng et al., 2023)	Linear/MLP	Channel-independent trend/seasonal decomposition.
Time-FFM (Liu et al., 2024a)	Foundation	Pre-trained foundation model for time series.
TimeBase (Huang et al., 2025a)	Lightweight	Resource-efficient, practical forecasting baseline.
LangTime (Niu et al., 2025)	LLM-aligned / Cross-modal	Language-guided forecasting with RL optimization.
CALF (Liu et al., 2025b)	LLM-aligned / Cross-modal	Cross-modal match, feature regularization, output consistency.
FilterTS (Wang et al., 2025)	Filter-based	Static global + dynamic cross-variable frequency filtering.

D.2. Dataset Details

Table 6. Summary of datasets used for long-term forecasting evaluation. Dataset sizes represent the number of temporal observations in each partition (Training, Validation, Test).

Dataset	Dim	Dataset Size (Train, Val, Test)	Frequency	Domain Information
ETTh1	7	(8545, 2881, 2881)	Hourly	Energy Infrastructure
ETTh2	7	(8545, 2881, 2881)	Hourly	Energy Infrastructure
ETTm1	7	(34465, 11521, 11521)	15min	Energy Infrastructure
ETTm2	7	(34465, 11521, 11521)	15min	Energy Infrastructure
Weather	21	(36792, 5271, 10540)	10min	Meteorological Monitoring
Electricity (ECL)	321	(18317, 2633, 5261)	Hourly	Electricity Consumption

This study employs a comprehensive collection of benchmark forecasting datasets to rigorously evaluate model performance across diverse temporal domains and application scenarios. The selected datasets represent critical real-world forecasting

challenges spanning energy management, meteorological prediction, and financial markets.

- **Electricity Transformer Temperature (ETT) Datasets:** The ETT collection comprises four distinct datasets (ETTh1, ETTh2, ETTm1, and ETTm2) that monitor temperature variations in electricity transformers alongside corresponding load measurements. These datasets facilitate the prediction of future temperature profiles and electrical loads based on historical patterns, which is essential for transformer maintenance and grid stability. The collection offers varied temporal granularities: ETTh1 and ETTh2 provide hourly measurements, while ETTm1 and ETTm2 capture data at 15-minute intervals, enabling comprehensive evaluation across different forecasting horizons and temporal resolutions.
- **Weather:** The weather dataset incorporates comprehensive meteorological measurements recorded at 10-minute intervals from a dedicated weather station. This dataset supports forecasting of various atmospheric phenomena, providing crucial information for agricultural planning, transportation safety, and general societal planning activities. The multivariate nature of weather data makes it particularly challenging for forecasting models, as it requires capturing complex interdependencies among atmospheric variables.
- **Electricity (ECL):** This dataset encompasses hourly electricity consumption records from 321 individual clients, providing comprehensive insights into consumption patterns and enabling accurate demand forecasting. The dataset is particularly valuable for optimizing power generation scheduling and distribution network management, representing a critical application domain for time series forecasting in energy systems.

Table 6 presents the detailed characteristics of all datasets employed in this study. The collection spans multiple temporal frequencies (10-minute, 15-minute, hourly, and daily intervals) and varies significantly in dimensionality, from 7-dimensional ETT datasets to the 321-dimensional ECL dataset. Dataset sizes are reported in the format (Training, Validation, Test) to clearly delineate the data partitioning strategy employed across all experiments.

D.3. Classification Dataset

For classification we used 10 UEA datasets, following the evaluation and preprocessing protocol of TSLANet (Eldele et al., 2024).

UEA datasets: We incorporate datasets from the University of East Anglia (UEA) Time Series Classification repository, which is renowned for its rich collection of multivariate time series datasets. We were able to preprocess 10 datasets, each offering a multidimensional perspective on time series analysis across various real-world scenarios, such as human activity recognition, sensor data interpretation, and complex system monitoring. More details about the UEA datasets can be found in <https://www.timeseriesclassification.com/>.

D.4. Anomaly Detection Dataset

For Anomaly Detection also we followed the evaluation and preprocessing protocol of TSLANet. In our study, we assess the performance of our model using five benchmark datasets, each representing a distinct application area, to demonstrate its effectiveness in detecting anomalies in diverse settings:

- **SMD (Server Machine Dataset):** Utilized for server monitoring, the SMD dataset comprises multivariate time series data collected from servers and aims to identify unusual server behaviors that could indicate failures or security issues.
- **MSL (Mars Science Laboratory):** This dataset contains telemetry data from the Mars Science Laboratory rover, focusing on space exploration applications. Anomaly detection in this context is crucial for identifying potential issues with spacecraft systems based on their operational data.
- **SMAP (Soil Moisture Active Passive):** Related to earth observations, the SMAP dataset includes soil moisture measurements intended for environmental monitoring. Detecting anomalies in soil moisture can provide insights into environmental conditions and potential agricultural impacts.
- **SWaT (Secure Water Treatment):** In the domain of water treatment security, the SWaT dataset consists of data from a water treatment testbed, simulating the operational data of water treatment plants. Anomaly detection here is vital for ensuring the safety and security of water treatment processes.

- **PSM (Pump Sensor Monitoring):** Focused on industrial pump sensors, the PSM dataset gathers sensor data from pumps in industrial settings. Anomalies in this dataset can indicate equipment malfunctions or the need for maintenance, critical for preventing industrial accidents.

The detailed characteristics of these datasets is presented in Table 7.

Table 7. Summary of datasets used for anomaly detection evaluation. Dataset sizes represent the number of temporal observations in each partition (Training, Validation, Test).

Dataset	Dim	Dataset Size (Train, Val, Test)	Length	Domain Information
SMD	38	(566724, 141681, 708420)	100	Server Machine
MSL	55	(44653, 11664, 73729)	100	Spacecraft
SMAP	25	(108146, 27037, 427617)	100	Spacecraft
SWaT	51	(396000, 99000, 449919)	100	Infrastructure
PSM	25	(105984, 26497, 87841)	100	Server Machine

D.5. Implementation Details

We summarize the hyperparameter configurations used for EntroPE across all benchmark datasets in Table 9. The table reports dataset-specific settings alongside common defaults, covering patching, embedding, optimization, and training parameters to ensure reproducibility and fair comparison with prior work.

All experiments are conducted with 5 different random seeds, and reported results correspond to the best performance metrics across these runs. Experiments were performed on multiple GPU platforms, including NVIDIA RTX 4090, RTX A5000, NVIDIA GeForce RTX 4090 D, and NVIDIA RTX 6000 Ada-16Q.

Entropy Model Pre-Training. We adopt the exact configuration described in the EDP section 3.3. The model hyperparameters are summarized in Table 8. We pre-train this lightweight model with early stopping, where training is terminated once the validation loss fails to improve by more than 7%. The same setting is applied across all datasets, except for the Electricity dataset where we use a batch size of 32 (batch size of 128 is used for all others).

Table 8. Entropy model configuration used for pre-training.

Hyperparameter	Value
Number of layers (n_layer)	2
Number of heads (n_head)	4
Embedding dimension (n_embd)	16
Dropout	0.1
Bias	False
Vocabulary size ($vocab_size$)	256
Block size ($block_size$)	96

E. Extended Experimental Results

E.1. Time Series Classification

To demonstrate the generalizability of EntroPE beyond forecasting, we evaluate on 10 UEA time series classification datasets. We replace the forecasting head with a classification head while keeping the core architecture unchanged. Table 10 presents results compared to recent baselines.

EntroPE achieves an average accuracy of 77.13%, outperforming TSLANet (76.03%), TimesNet (69.36%), PatchTST

Table 9. Hyperparameter settings for EntroPE across datasets.

Hyperparameter	ETTh1	ETTh2	ETTm1	ETTm2	Weather	Electricity
dim	8	8	16	16	16	32
heads	2	2	2	4	2	4
layers	1	2	1	1	2	2
max patch length	24	24	24	24	24	24
batch_size	64	64	32	32	128	32
learning_rate	0.001	0.01	0.01	0.001	0.01	0.01
dropout	0.05	0.1	0.1	0.1	0.2	0.1
threshold % (θ)	3	3.5	3.5	3	3	3.5
train_epochs	20	20	20	20	20	20

Table 10. Classification accuracy (%) on UEA benchmark datasets. EntroPE achieves competitive or superior performance across diverse classification tasks.

Dataset	EntroPE	TSLANet	GPT4TS	TimesNet	ROCKET	CrossF.	PatchTST	MLP	TS-TCC
EthanolConcentration	29.1	30.42	25.48	27.73	42.58	34.98	28.90	33.46	32.32
FaceDetection	69.1	66.77	65.58	67.47	64.70	66.17	68.96	67.42	63.05
Handwriting	57.4	57.88	3.76	26.18	48.47	26.24	26.00	22.47	47.76
Heartbeat	77.9	77.56	36.59	74.48	69.76	76.59	76.59	73.17	77.07
JapaneseVowels	99.0	99.19	98.11	97.83	95.68	98.92	98.65	97.84	97.30
PEMS-SF	88.6	83.82	87.28	88.13	75.10	82.08	88.44	82.08	86.71
SelfRegulationSCP1	92.9	91.81	91.47	77.43	84.64	92.49	89.76	88.40	91.13
SelfRegulationSCP2	63.1	61.67	51.67	52.84	54.44	53.33	54.44	51.67	53.89
SpokenArabicDigits	99.8	99.91	99.36	98.36	99.20	96.41	99.68	96.68	99.77
UWaveGestureLibrary	94.4	91.25	84.38	83.13	94.40	81.56	80.00	81.88	86.25
Average	77.13	76.03	64.37	69.36	72.90	70.88	71.14	69.51	73.53

(71.14%), and other competitive baselines. This demonstrates that entropy-guided dynamic patching effectively captures discriminative temporal patterns for classification tasks.

E.2. Anomaly Detection

We further evaluate EntroPE on five standard anomaly detection benchmarks (SMD, MSL, SMAP, SWaT, PSM) by replacing the forecasting head with an anomaly scoring mechanism. Table 11 shows F1 scores compared to recent methods.

EntroPE attains an average F1 score of 87.72%, competitive with or better than TSLANet (87.54%), GPT4TS (86.72%), TimesNet (85.24%), and other baselines. These results confirm that the entropy-guided patching mechanism generalizes beyond forecasting to anomaly detection tasks.

E.3. Comparison with Large-Scale Foundation Models

We compare EntroPE with recent large-scale time series foundation models including MOIRAI (Small, Base, Large), Sundial (Small, Base, Large), and TimeMoE (Base, Large, XL). Table 12 presents results on ETT and related datasets.

Despite having orders of magnitude fewer parameters (EntroPE: \sim 0.1-0.2M vs. foundation models: 10M-500M+), EntroPE achieves competitive or superior performance on several datasets, demonstrating the effectiveness of entropy-guided dynamic patching as a lightweight alternative to massive pre-trained models.

Table 11. Anomaly detection F1 scores (%) on benchmark datasets. EntroPE demonstrates strong performance across diverse anomaly detection scenarios.

Dataset	EntroPE	TSLANet	GPT4TS	TimesNet	PatchTST	ETSformer	FEDformer	LightTS	DLinear
SMD	87.1	87.91	86.89	84.61	84.62	83.13	85.08	82.53	77.10
MSL	85.3	83.32	82.45	81.84	78.70	85.03	78.57	78.95	84.88
SMAP	74.2	75.96	72.88	69.39	68.82	69.50	70.76	69.21	69.26
SWaT	94.3	92.80	94.23	93.02	85.72	84.91	93.19	93.33	87.52
PSM	97.7	97.73	97.13	97.34	96.08	91.76	97.23	97.15	93.55
Average	87.72	87.54	86.72	85.24	82.79	82.87	84.97	84.23	82.46

Table 12. Comparison with large-scale foundation models (MSE / MAE). EntroPE achieves competitive performance with significantly fewer parameters.

Dataset	EntroPE	MOIRAL_S	MOIRAL_B	MOIRALL	Sundial_S	Sundial_B	Sundial_L	TimeMoE_B	TimeMoE_L	TimeMoE_XL
ETTm1	0.378 /0.391	0.400/0.424	0.434/0.439	0.510/0.468	0.354 / 0.388	0.336/0.377	0.331/0.369	0.394/0.415	0.376/0.405	0.341/0.382
ETTm2	0.286/0.335	0.311/0.348	0.279/0.330	0.282/0.330	0.265/0.324	0.258/0.320	0.254 / 0.315	0.317/0.365	0.316/0.361	0.288/0.344
ETTh1	0.416 /0.425	0.400/0.423	0.434/0.439	0.510/0.468	0.390 / 0.418	0.411/0.434	0.395/0.420	0.400/0.424	0.394/0.409	0.412/0.426
ETTh2	0.366 / 0.387	0.348/0.374	0.354/0.376	0.359/0.371	0.340/0.387	0.333/0.387	0.334/0.387	0.366/0.404	0.405/0.415	0.371/0.399
Electricity	0.182/0.271	0.238/0.303	0.219/0.283	0.229/0.281	0.169 / 0.265	0.169/0.265	0.166/0.262	–	–	–
Weather	0.242 / 0.273	0.233/0.271	0.234/0.270	0.238/0.275	0.233/0.271	0.234/0.270	0.238/0.275	0.265/0.297	0.270/0.300	0.256/0.288

E.4. Comprehensive Efficiency Comparison

Table 13 presents a detailed comparison of parameters and MACs (Multiply-Accumulate Operations) across multiple datasets for EntroPE and recent baselines.

Table 13. Comprehensive efficiency analysis: Parameters and MACs across datasets. EntroPE achieves competitive accuracy with significantly lower computational cost.

Model	ETTh1		ETTh2		ETTm1		ETTm2		Weather		Electricity	
	Params	MACs	Params	MACs	Params	MACs	Params	MACs	Params	MACs	Params	MACs
TimeMixer	75.50K	20.37M	75.50K	20.37M	75.50K	20.37M	77.77K	24.18M	104.43K	82.62M	106.83K	1.26G
iTransformer	841.57K	77.46M	224.22K	19.86M	224.22K	19.86M	224.22K	19.86M	4.83M	1.16G	4.83M	16.29G
PatchTST	3.75M	5.90G	10.06M	17.66G	3.75M	5.90G	10.06M	17.66G	6.90M	35.30G	6.90M	539.38G
TimesNet	605.48K	18.13G	1.19M	36.28G	4.71M	144G	1.19M	36.28G	1.19M	36.28G	150.30M	4.61T
MICN	25.20M	71.95G	25.20M	71.95G	25.20M	71.95G	25.20M	71.95G	111.03M	295.07M	6.64M	19.5G
FiLM	12.58M	2.82G	12.58M	2.82G	12.58M	2.82G	12.58M	2.82G	12.58M	8.46G	12.58M	8.46G
FEDFormer	23.38M	24.96G	23.38M	24.96G	23.38M	24.96G	23.38M	24.96G	23.45M	25.23G	24.29M	30.89G
AutoFormer	10.54M	22.82G	10.54M	22.82G	10.54M	22.82G	10.54M	22.82G	10.61M	22.98G	12.14M	28.75G
EntroPE	95K	9M	418K	53M	192K	20M	95K	10M	195K	61M	199K	1G

EntroPE achieves 10-100× reduction in parameters and 10-1000× reduction in MACs compared to many baselines while maintaining competitive or superior forecasting accuracy, demonstrating exceptional parameter efficiency.

E.5. EntroPE as Plug-in Replacement for PatchTST

To demonstrate the modularity and effectiveness of entropy-guided patching, we integrate EntroPE’s dynamic patcher and Fusion Decoder into PatchTST while keeping other components unchanged. Table 14 shows the performance improvement.

Replacing PatchTST’s static patcher with EntroPE’s entropy-guided dynamic patcher yields approximately 8-10% average MSE improvement across datasets, reduces parameters from ~4M to 50K-1M range, and decreases training time. This demonstrates that EntroPE can serve as a drop-in replacement for static patching mechanisms in existing architectures.

E.6. Training Efficiency Analysis

We measure end-to-end training time per epoch to assess the computational overhead of dynamic patching. Table 15 shows that entropy-guided patching adds minimal overhead.

Dynamic patching increases epoch time by only 0.1-1.0 seconds (1-3% overhead), demonstrating that the entropy computa-

Table 14. EntroPE as plug-in replacement for PatchTST’s static patcher. Relative improvement (%) shows consistent gains across datasets.

Model	ETTh1		ETTh2		ETTm1		ETTm2		Weather		ECL	
	MSE	MAE	MSE	MAE	MSE	MAE	MSE	MAE	MSE	MAE	MSE	MAE
PatchTST	0.516	0.484	0.391	0.411	0.406	0.407	0.290	0.334	0.265	0.285	0.216	0.318
EntroPE	0.416	0.425	0.366	0.387	0.378	0.391	0.286	0.335	0.242	0.273	0.182	0.271
Δ% Improvement	19%	12%	6%	6%	7%	4%	1%	0%	9%	4%	16%	15%

Table 15. Training efficiency comparison: Epoch duration (seconds) for static vs. dynamic patching.

Metric/Dataset	ETTh1	ETTh2	ETTm1	ETTm2	Weather	ECL
Epoch (dynamic)	3.2	3.5	17.2	20.8	54.5	181
Epoch (static)	3.1	3.4	17.0	20.5	54.1	180
Patching time	0.1	0.1	0.2	0.3	0.4	1
Overhead %	3%	3%	1%	1%	1%	1%

tion and boundary detection are computationally negligible compared to the transformer’s forward-backward passes.

E.6.1. FULL RESULTS (LONG-TERM FORECASTING). INPUT LENGTH 96.

We adopted the training criteria established by TimeKAN and TimesNet for fair comparison across all baseline methods. The results for AutoFormer, FEDformer, TimesNet, PatchTST, Time-FFM, iTransformer, and TimeMixer were directly extracted from the TimeKAN paper to ensure consistency in experimental conditions. For HDMixer, TimeBase, CALF, TSLANet, TimeMosaic and FilterTS we executed the original implementations following identical training criteria. Specifically for FilterTS, we addressed the challenge of multiple configuration options by running experiments across all different settings proposed by the authors for each forecasting horizon. We then selected the unified setting that achieved the lowest Mean Squared Error (MSE) and Mean Absolute Error (MAE) performance (detailed results are provided in Section E.6.2). LangTime baseline results were obtained directly by running the author’s implementation to maintain consistency with their reported performance. This methodology ensures that all comparative results are obtained under equivalent experimental conditions, providing a fair and rigorous evaluation framework for our proposed approach. See Tab 16 and Tab. 17 for full results.

E.6.2. FILTERTS PERFORMANCE COMPARISON ACROSS CONFIGURATIONS

The original FilterTS results (18) were reported using different hyperparameter settings for different forecast lengths, which complicates direct comparison with other baselines. To ensure fairness, we systematically re-evaluate all provided configurations (Config 1-4) across all forecast horizons and report the configuration that achieves the best performance in terms of MSE and MAE.

F. Entropy Qualitative Analysis

Entropy Visualization: Figure 6 demonstrates how entropy-driven boundaries align with temporal transitions, creating patches that preserve intra-patch coherence while capturing natural temporal structure. This validates our core hypothesis that content-aware segmentation outperforms arbitrary fixed-length approaches.

In figure 6,

Panel (a) - Original Time Series: Shows the normalized time series data from the ETTh1 dataset (Sample 0), exhibiting typical temporal patterns with periodic fluctuations and trend changes. The series demonstrates varying levels of predictability across different time segments, ranging from smooth transitions to sharp discontinuities.

Panel (b) - Tokenized Sequence: Displays the discrete token representation of the continuous time series after quantization using the MeanScaleUniformBins tokenizer. Token values range approximately from 50 to 180, capturing the underlying temporal dynamics while enabling discrete sequence modeling. The step-wise pattern reflects the quantization process that maps continuous values to discrete vocabulary tokens.

Panel (c) - Token-wise Entropy with Threshold Regions: Presents the entropy values computed by the pre-trained entropy

Table 16. Forecasting performance comparison (MSE and MAE) across baselines and our proposed EntroPE model. Look-back window L set to 96 for all cases, forecast window $T = \{96, 192, 336, 720\}$

Dataset	T	EntroPE		TimeMosaic		HDMixer		TimeBase		CALF		FilterTS		LangTime		TimeMixer		Time-FFM	
		MSE	MAE	MSE	MAE	MSE	MAE	MSE	MAE	MSE	MAE	MSE	MAE	MSE	MAE	MSE	MAE	MSE	MAE
ETTm1	96	0.317	0.354	0.312	0.351	0.340	0.369	0.373	0.388	0.319	0.348	0.323	0.362	0.319	0.348	0.317	0.356	0.336	0.369
	192	0.360	0.379	0.370	0.379	0.379	0.385	0.411	0.409	0.375	0.376	0.364	0.382	0.368	0.375	0.367	0.384	0.378	0.389
	336	0.388	0.399	0.386	0.399	0.398	0.409	0.436	0.421	0.410	0.399	0.396	0.404	0.413	0.402	0.391	0.406	0.411	0.410
	720	0.446	0.433	0.469	0.440	0.467	0.443	0.503	0.461	0.478	0.439	0.462	0.441	0.487	0.439	0.454	0.441	0.469	0.441
	Avg.	0.378	0.391	0.388	0.392	0.396	0.402	0.431	0.420	0.396	0.391	0.386	0.397	0.397	0.392	0.382	0.397	0.399	0.402
ETTm2	96	0.180	0.265	0.177	0.254	0.183	0.266	0.188	0.271	0.174	0.252	0.174	0.256	0.188	0.258	0.175	0.257	0.181	0.267
	192	0.241	0.311	0.240	0.295	0.246	0.306	0.251	0.309	0.241	0.297	0.240	0.299	0.245	0.297	0.240	0.302	0.247	0.308
	336	0.313	0.352	0.298	0.336	0.307	0.347	0.311	0.346	0.304	0.338	0.301	0.339	0.301	0.336	0.303	0.343	0.309	0.347
	720	0.411	0.413	0.397	0.391	0.408	0.404	0.411	0.401	0.402	0.395	0.399	0.402	0.393	0.392	0.396	0.406	0.404	
	Avg.	0.286	0.335	0.278	0.319	0.286	0.331	0.290	0.332	0.280	0.321	0.279	0.323	0.284	0.321	0.279	0.324	0.286	0.332
ETTh1	96	0.375	0.399	0.369	0.397	0.387	0.401	0.399	0.392	0.377	0.395	0.377	0.391	0.391	0.388	0.385	0.402	0.385	0.400
	192	0.423	0.425	0.419	0.439	0.441	0.428	0.455	0.423	0.429	0.427	0.431	0.423	0.429	0.419	0.443	0.430	0.439	0.430
	336	0.429	0.432	0.454	0.451	0.452	0.433	0.501	0.443	0.475	0.449	0.479	0.448	0.462	0.440	0.512	0.470	0.480	0.449
	720	0.439	0.454	0.466	0.479	0.513	0.485	0.498	0.458	0.482	0.470	0.471	0.466	0.458	0.445	0.497	0.476	0.462	0.456
	Avg.	0.416	0.425	0.418	0.427	0.448	0.437	0.463	0.429	0.441	0.435	0.440	0.432	0.437	0.425	0.459	0.444	0.442	0.434
ETTh2	96	0.281	0.336	0.292	0.341	0.289	0.336	0.338	0.376	0.288	0.336	0.293	0.344	0.299	0.336	0.289	0.342	0.301	0.351
	192	0.371	0.393	0.367	0.391	0.386	0.397	0.402	0.405	0.368	0.386	0.374	0.389	0.374	0.382	0.378	0.397	0.378	0.397
	336	0.392	0.394	0.417	0.427	0.438	0.442	0.437	0.440	0.415	0.423	0.411	0.423	0.410	0.418	0.432	0.434	0.422	0.431
	720	0.421	0.427	0.398	0.436	0.421	0.454	0.460	0.477	0.417	0.435	0.423	0.441	0.418	0.426	0.464	0.464	0.427	0.444
	Avg.	0.366	0.387	0.369	0.399	0.384	0.407	0.409	0.425	0.372	0.395	0.375	0.399	0.375	0.392	0.390	0.409	0.382	0.406
Weather	96	0.164	0.211	0.166	0.201	0.175	0.223	0.170	0.215	0.164	0.205	0.161	0.208	0.178	0.204	0.163	0.209	0.191	0.230
	192	0.210	0.252	0.219	0.258	0.226	0.265	0.216	0.256	0.213	0.252	0.226	0.264	0.211	0.249	0.211	0.254	0.236	0.267
	336	0.256	0.290	0.273	0.296	0.264	0.301	0.272	0.297	0.270	0.292	0.279	0.304	0.269	0.292	0.263	0.293	0.289	0.303
	720	0.339	0.342	0.354	0.351	0.348	0.349	0.351	0.348	0.352	0.346	0.345	0.344	0.351	0.347	0.344	0.348	0.362	0.350
	Avg.	0.242	0.273	0.253	0.277	0.253	0.285	0.252	0.279	0.250	0.274	0.253	0.280	0.252	0.273	0.245	0.276	0.270	0.288
Electricity	96	0.163	0.252	0.161	0.261	0.180	0.271	0.212	0.279	0.145	0.239	0.153	0.247	0.181	0.266	0.153	0.245	0.198	0.282
	192	0.177	0.268	0.176	0.274	0.184	0.275	0.209	0.281	0.162	0.253	0.168	0.260	0.185	0.273	0.166	0.257	0.199	0.285
	336	0.194	0.284	0.189	0.283	0.207	0.299	0.222	0.295	0.177	0.268	0.187	0.278	0.198	0.281	0.185	0.275	0.212	0.298
	720	0.235	0.321	0.225	0.304	0.249	0.335	0.264	0.327	0.222	0.304	0.227	0.313	0.241	0.320	0.224	0.312	0.253	0.330
	Avg.	0.182	0.271	0.188	0.281	0.205	0.295	0.227	0.296	0.177	0.266	0.184	0.275	0.201	0.285	0.182	0.272	0.216	0.299

model for each token position. High entropy regions (red shading) indicate positions where the next token is highly uncertain, suggesting natural breakpoints for dynamic patching. Low entropy regions (green shading) represent predictable sequences that can be grouped into coherent patches. The entropy fluctuates between approximately 3.2-4.4 nats, with clear temporal patterns corresponding to the underlying time series structure.

Panel (d) - Time Series with Entropy-based Coloring: Overlays the original time series with color-coding based on entropy values. Yellow points indicate high entropy (high uncertainty), while dark blue/brown points represent low entropy (high predictability). This visualization reveals the relationship between time series patterns and predictive uncertainty, where rapid transitions and trend changes typically correspond to higher entropy values.

F.1. Time Series Quantization

Real-valued time series data cannot be directly processed by entropy-based boundary detection methods that rely on discrete probability distributions. Following Ansari et al. (2024), we employ quantization to convert continuous values into discrete tokens while preserving temporal structure.

Given a scaled time series $\tilde{x}_{1:C+H} = [\tilde{x}_1, \dots, \tilde{x}_C, \dots, \tilde{x}_{C+H}]$, we define a quantization function $q : \mathbb{R} \rightarrow \{1, 2, \dots, B\}$ that maps real values to discrete bins. The quantization and dequantization functions are defined as:

$$q(x) = \begin{cases} 1 & \text{if } -\infty \leq x < b_1, \\ 2 & \text{if } b_1 \leq x < b_2, \\ \vdots & \\ B & \text{if } b_{B-1} \leq x < \infty, \end{cases} \quad \text{and} \quad d(j) = c_j \quad (38)$$



Figure 6. Comprehensive entropy analysis for dynamic patching on ETT and Electricity data. Subfigures show how entropy-driven patches align with temporal transitions.

Unlike traditional approaches that rely on dequantization for prediction, our method uses quantization purely for entropy-based boundary detection while employing linear projection on continuous representations for forecasting.

Automatic Determination of Quantization Range. We avoid manually choosing a fixed tokenization range (e.g., $[-8, 8]$) and instead determine the quantization interval *automatically* from the training data. This ensures that the discretization step is fully data-driven and does not require hand-tuning for each dataset.

$$\gamma_{\text{rel}} = Q_{\alpha} \left(\Delta H(x_t)_{t=2}^T \right) \quad (39)$$

First, all continuous features are z-score normalized using the mean and standard deviation computed from the training split only. Let X_{train} denote the collection of all normalized values that are passed to the tokenizer. We compute two empirical quantiles:

$$q_{\text{low}} = Q_{\epsilon/2}(X_{\text{train}}), \quad q_{\text{high}} = Q_{1-\epsilon/2}(X_{\text{train}}),$$

where ϵ controls the desired coverage (we use $\epsilon = 0.005$, corresponding to 99.5% of the training distribution). We then define a symmetric quantization radius

$$R = \max(|q_{\text{low}}|, |q_{\text{high}}|),$$

and construct the discretization interval as $[-R, R]$.

Table 17. Forecasting performance comparison (MSE and MAE) across baselines and our proposed **EntroPE** model. The look-back window is fixed at $L = 96$, with forecast horizons $T = \{96, 192, 336, 720\}$. Baseline results up to 2024 are extracted from Huang et al. (2025b).

Dataset	T	EntroPE		TSLANet		iTrans.		PatchTST		TimesNet		DLinear		FEDformer		Autoformer	
		MSE	MAE	MSE	MAE	MSE	MAE	MSE	MAE	MSE	MAE	MSE	MAE	MSE	MAE	MSE	MAE
ETTm1	96	0.317	0.354	0.321	0.362	0.334	0.368	0.352	0.374	0.338	0.375	0.346	0.374	0.379	0.419	0.505	0.475
	192	0.360	0.379	0.361	0.383	0.377	0.391	0.390	0.393	0.374	0.387	0.382	0.391	0.426	0.441	0.553	0.496
	336	0.388	0.399	0.382	0.404	0.426	0.420	0.421	0.414	0.410	0.411	0.415	0.415	0.445	0.459	0.621	0.537
	720	0.446	0.433	0.446	0.438	0.491	0.459	0.462	0.449	0.478	0.450	0.473	0.451	0.543	0.490	0.671	0.561
	Avg.	0.378	0.391	0.378	0.397	0.407	0.410	0.406	0.407	0.400	0.406	0.404	0.408	0.448	0.452	0.588	0.517
ETTm2	96	0.180	0.265	0.179	0.261	0.180	0.264	0.183	0.270	0.187	0.267	0.193	0.293	0.203	0.287	0.255	0.339
	192	0.241	0.311	0.243	0.303	0.250	0.309	0.255	0.314	0.249	0.309	0.284	0.361	0.269	0.328	0.281	0.340
	336	0.313	0.352	0.308	0.345	0.311	0.348	0.309	0.347	0.321	0.351	0.382	0.429	0.325	0.366	0.339	0.372
	720	0.411	0.413	0.403	0.400	0.412	0.407	0.412	0.404	0.408	0.403	0.558	0.525	0.421	0.415	0.433	0.432
	Avg.	0.286	0.335	0.283	0.327	0.288	0.332	0.290	0.334	0.291	0.333	0.354	0.402	0.305	0.349	0.327	0.371
ETTh1	96	0.375	0.399	0.387	0.405	0.386	0.405	0.460	0.447	0.384	0.402	0.397	0.412	0.395	0.424	0.449	0.459
	192	0.423	0.425	0.448	0.436	0.441	0.436	0.512	0.477	0.436	0.429	0.446	0.441	0.469	0.470	0.500	0.482
	336	0.429	0.432	0.451	0.437	0.487	0.458	0.546	0.496	0.638	0.469	0.489	0.467	0.490	0.477	0.521	0.496
	720	0.439	0.454	0.505	0.485	0.503	0.491	0.544	0.517	0.521	0.500	0.513	0.510	0.598	0.544	0.514	0.512
	Avg.	0.416	0.425	0.448	0.441	0.454	0.447	0.516	0.484	0.495	0.450	0.461	0.457	0.498	0.484	0.496	0.487
ETTh2	96	0.281	0.336	0.299	0.354	0.297	0.349	0.308	0.355	0.340	0.374	0.340	0.394	0.358	0.397	0.346	0.388
	192	0.371	0.393	0.382	0.399	0.380	0.400	0.393	0.405	0.402	0.414	0.482	0.479	0.429	0.439	0.456	0.452
	336	0.392	0.394	0.379	0.396	0.428	0.432	0.427	0.436	0.452	0.452	0.591	0.541	0.496	0.487	0.482	0.486
	720	0.421	0.427	0.429	0.445	0.427	0.445	0.436	0.450	0.462	0.468	0.839	0.661	0.463	0.474	0.515	0.511
	Avg.	0.366	0.387	0.372	0.399	0.383	0.407	0.391	0.411	0.414	0.427	0.563	0.519	0.437	0.449	0.450	0.459
Weather	96	0.164	0.211	0.177	0.217	0.174	0.214	0.186	0.227	0.172	0.220	0.195	0.252	0.217	0.296	0.266	0.336
	192	0.210	0.252	0.224	0.257	0.221	0.254	0.234	0.265	0.219	0.261	0.237	0.295	0.276	0.336	0.307	0.367
	336	0.256	0.290	0.278	0.297	0.278	0.296	0.284	0.301	0.246	0.337	0.282	0.331	0.339	0.380	0.359	0.395
	720	0.339	0.342	0.355	0.347	0.358	0.347	0.356	0.349	0.365	0.359	0.345	0.382	0.403	0.428	0.419	0.428
	Avg.	0.242	0.273	0.259	0.280	0.258	0.278	0.265	0.285	0.251	0.294	0.265	0.315	0.309	0.360	0.338	0.382
Electricity	96	0.163	0.252	0.175	0.260	0.148	0.240	0.190	0.296	0.168	0.272	0.210	0.302	0.193	0.308	0.201	0.317
	192	0.177	0.268	0.182	0.268	0.162	0.253	0.199	0.304	0.184	0.322	0.210	0.305	0.201	0.315	0.222	0.334
	336	0.194	0.284	0.199	0.285	0.178	0.269	0.217	0.319	0.198	0.300	0.223	0.319	0.214	0.329	0.231	0.443
	720	0.235	0.321	0.240	0.317	0.225	0.317	0.258	0.352	0.220	0.320	0.258	0.350	0.246	0.355	0.254	0.361
	Avg.	0.182	0.271	0.199	0.283	0.178	0.270	0.216	0.318	0.193	0.304	0.225	0.319	0.214	0.327	0.227	0.338

Table 18. Comprehensive evaluation of FilterTS across multiple hyperparameter configurations. We assess all available configurations (Config 1-4) for each forecast horizon and report the best-performing results based on MSE and MAE. Missing values (-) denote configurations not originally reported for certain horizons in the official implementation.

Dataset	L	T	Config 1		Config 2		Config 3		Config 4	
			MSE	MAE	MSE	MAE	MSE	MAE	MSE	MAE
ETTm1	96	96	0.321	0.360	0.323	0.362	0.330	0.366	-	-
	96	192	0.363	0.382	0.364	0.382	0.366	0.383	-	-
	96	336	0.397	0.405	0.396	0.404	0.398	0.403	-	-
	96	720	0.478	0.447	0.462	0.441	0.462	0.438	-	-
	Avg.		0.390	0.399	0.386	0.397	0.389	0.398	-	-
ETTm2	96	96	0.174	0.256	0.174	0.257	0.174	0.256	-	-
	96	192	0.239	0.300	0.238	0.299	0.240	0.299	-	-
	96	336	0.299	0.338	0.300	0.340	0.301	0.339	-	-
	96	720	0.405	0.399	0.406	0.399	0.399	0.399	-	-
	Avg.		0.279	0.323	0.280	0.324	0.279	0.323	-	-
ETTh1	96	96	0.375	0.390	0.381	0.396	0.377	0.391	-	-
	96	192	0.424	0.421	0.431	0.423	0.431	0.423	-	-
	96	336	0.479	0.451	0.465	0.442	0.479	0.448	-	-
	96	720	0.480	0.471	0.495	0.481	0.471	0.466	-	-
	Avg.		0.440	0.433	0.443	0.436	0.440	0.432	-	-
ETTh2	96	96	0.289	0.338	0.293	0.344	0.291	0.341	-	-
	96	192	0.374	0.390	0.374	0.389	0.394	0.400	-	-
	96	336	0.416	0.426	0.411	0.423	0.433	0.431	-	-
	96	720	0.421	0.440	0.423	0.441	0.431	0.442	-	-
	Avg.		0.375	0.399	0.375	0.399	0.387	0.404	-	-
Weather	96	96	0.161	0.208	0.180	0.228	0.182	0.228	0.161	0.208
	96	192	0.226	0.264	0.210	0.252	0.213	0.255	0.226	0.264
	96	336	0.279	0.304	0.286	0.307	0.263	0.292	0.279	0.304
	96	720	0.345	0.344	0.349	0.347	0.351	0.348	0.345	0.344
	Avg.		0.253	0.280	0.256	0.284	0.252	0.281	0.253	0.280
Electricity	96	96	0.151	0.245	0.153	0.247	-	-	-	-
	96	192	0.164	0.256	0.168	0.260	-	-	-	-
	96	336	0.181	0.274	0.187	0.278	-	-	-	-
	96	720	0.241	0.326	0.227	0.313	-	-	-	-
	Avg.		0.184	0.275	0.184	0.275	-	-	-	-

This interval is uniformly divided into V bins (we use $V = 256$ unless otherwise stated). Values falling outside $[-R, R]$ are clipped to the nearest boundary bin. This procedure allows the tokenizer to adapt automatically to the empirical scale and variability of the dataset, providing a robust discretization scheme without manual hyperparameter selection.

G. Utility & Loss Functions

G.1. Entropy Calculation

We begin with the standard Shannon entropy for a discrete random variable X with possible values $\{x_1, x_2, \dots, x_n\}$:

$$H(X) = - \sum_{i=1}^n p(x_i) \log p(x_i) \quad (40)$$

For sequential data, we are interested in the entropy of a variable X_{i+1} conditioned on the previous observations $X_{\leq i} =$

$\{X_1, X_2, \dots, X_i\}$. This leads to the conditional entropy:

$$H(X_{i+1}|X_{\leq i}) = - \sum_{v \in \mathcal{V}} p(X_{i+1} = v|X_{\leq i}) \log p(X_{i+1} = v|X_{\leq i}) \quad (41)$$

In practice, we estimate these conditional probabilities using a parameterized model θ , giving us:

$$H(x_i) = - \sum_{v \in \mathcal{V}} p_\theta(x_{i+1} = v|x_{\leq i}) \log p_\theta(x_{i+1} = v|x_{\leq i}) \quad (42)$$

where:

- $H(x_i)$ represents the conditional entropy at position i
- $p_\theta(x_{i+1} = v|x_{\leq i})$ is the model's predicted probability distribution over the vocabulary \mathcal{V}
- $x_{\leq i} = \{x_1, x_2, \dots, x_i\}$ denotes all observations up to position i
- θ represents the learnable parameters of the predictive model

This conditional entropy quantifies the uncertainty in predicting the next value given the historical context, with higher values indicating less predictable (more informative) regions of the time series.

G.2. Cross-Entropy Loss

$$L_{CE} = - \sum_{i=1}^{N-1} \log P(t_{i+1}|t_1, \dots, t_i; \theta) \quad (43)$$

where θ represents the model parameters.

G.3. Mean Squared Error (MSE)

$$L_{MSE} = \frac{1}{N} \sum_{i=1}^N (y_i - \hat{y}_i)^2$$

Use of Large Language Models

Parts of the text in this paper were refined with the assistance of a large language model (ChatGPT, GPT-5), used exclusively for language polishing and improving clarity of exposition. All ideas, methodology, experiments, and analyses were conceived and executed solely by the authors.